Joana Andreia Casanova Ferreira Alves

Licenciada em Ciências de Engenharia Física

Characterization of an OPCPA laser amplifier based on the nonlinear crystal YCOB

Dissertação para obtenção do Grau de Mestre em
Engenharia Física

Orientadores: Ana Gomes Silva, Professora Auxiliar, FCT-UNL

Gonçalo Figueira, Professor Auxiliar, IST-UL

Júri:

Presidente: Isabel Catarino,
Professora Auxiliar,
FCT-UNL

Arguentes: Dawei Liang,
Professor Auxiliar,
FCT-UNL

Vogais: Gonçalo Figueira,
Professor Auxiliar,
IST-UL

FACULDADE DE
CIÊNCIAS E TECNOLOGIA
UNIVERSIDADE NOVA DE LISBOA

Março, 2015

Characterization of an OPCPA laser amplifier based on the nonlinear crystal YCOB

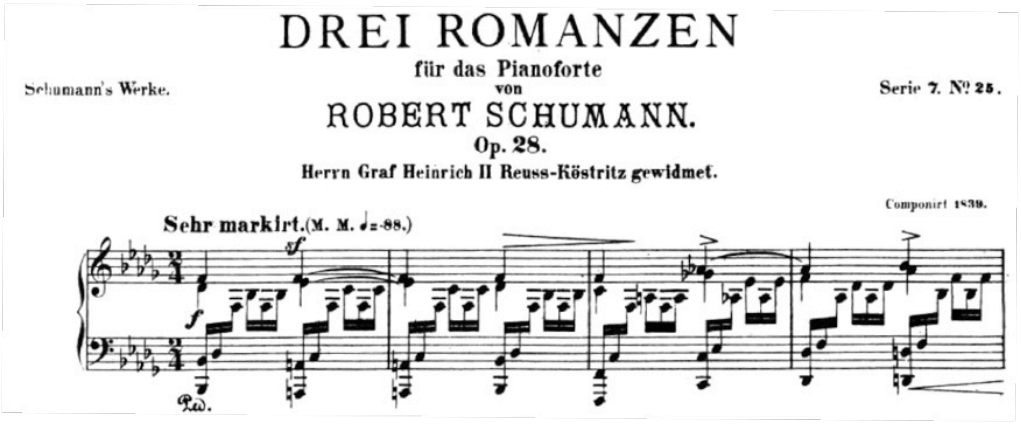

DREI ROMANZEN

für das Pianoforte

von

ROBERT SCHUMANN.

Op. 28.

Herrn Graf Heinrich II Reuss-Köstritz gewidmet.

Schumann's Werke.

Serie 7. № 25.

Componirt 1839.

Sehr markirt. (M. M. ♩= 88.)

Agradecimentos

Antes de mais gostaria de agradecer aos meus orientadores por me terem dado a oportunidade única de trabalhar numa área tão interessante e desafiante como a óptica e os fenómenos associados à produção de sistemas laser intensos; à Professora Ana Gomes Silva por ter estabelecido esta colaboração e ao Professor Gonçalo Figueira por me ter acolhido de forma tão agradável e simpática no seu grupo. Agradeço a ambos, de igual modo, o apoio imprescindível ao longo de todo o trabalho incluindo a fase de preparação de dissertação, a orientação sabedora bem como as sugestões para o desenvolvimento deste trabalho, no esclarecimento de dúvidas e discussões científicas. Não menos importante foi a sua total disponibilidade e incentivo permanente à descoberta das minhas perspectivas futuras. A amizade demonstrada e o conhecimento transmitido foram de uma grande inspiração e motivação para mim.

No entanto, não poderia também deixar de agradecer ao Celso João por ter acompanhado todo o meu trabalho experimental e teórico assim como pelas longas discussões e esclarecimentos que paciente e alegremente prestou até ao surgimento das soluções. Ao Hugo Pires por ter contribuído para a minha melhor compreensão sobre os conceitos não lineares do amplificador paramétrico, bem como pelas histórias bem contadas que divertiam o grupo durante as longas horas de trabalho no laboratório.

Agradeço ao IPFN por me ter disponibilizado os meios necessários à realização do trabalho nas melhores condições e a todos os elementos do GoLP em especial alunos, técnicos, professores e funcionários por me terem recebido calorosamente.

Para finalizar, o apoio incondicional da minha família, dos meus amigos e a minha música, foram essenciais e imprescindíveis para a conclusão de um percurso tão marcante e por isso o meu obrigado a todos, todos, mas mesmo a todos eles.

Abstract

The work described in this thesis was performed at the Laboratory for Intense Lasers (L2I) of Instituto Superior Técnico, University of Lisbon (IST-UL). Its main contribution consists in the feasibility study of the broadband dispersive stages for an optical parametric chirped pulse amplifier based on the nonlinear crystal yttrium calcium oxi-borate (YCOB). In particular, the main goal of this work consisted in the characterization and implementation of the several optical devices involved in pulse expansion and compression of the amplified pulses to durations of the order of a few optical cycles (20 fs). This type of laser systems find application in fields such as medicine, telecommunications and machining, which require high energy, ultrashort (sub-100 fs) pulses.

The main challenges consisted in the preliminary study of the performance of the broadband amplifier, which is essential for successfully handling pulses with bandwidths exceeding 100 nm when amplified from the μJ to 20 mJ per pulse. In general, the control, manipulation and characterization of optical phenomena on the scale of a few tens of fs and powers that can reach the PW level are extremely difficult and challenging due to the complexity of the phenomena of radiation-matter interaction and their nonlinearities, observed at this time scale and power level.

For this purpose the main dispersive components were characterized in detail, specifically addressing the demonstration of pulse expansion and compression. The tested bandwidths are narrower than the final ones, in order to confirm the parameters of these elements and predict the performance for the broadband pulses. The work performed led to additional tasks such as a detailed characterization of laser oscillator seeding the laser chain and the detection and cancelling of additional sources of dispersion.

Keywords: Optical parametric chirped-pulse amplification; Ultra-short laser pulses; Pulse diagnostics; Pulse compression; Optical dispersion.

Resumo

O trabalho descrito nesta dissertação foi realizado no Laboratório de Lasers Intensos (L2I) do Instituto Superior Técnico da Universidade de Lisboa (IST/UL), tendo contribuído para o desenvolvimento de um amplificador laser, do tipo amplificação óptica paramétrica de impulsos dispersos baseado num cristal não-linear de oxi-borato de ítrio-cálcio (YCOB). Em particular, o principal objectivo deste trabalho consistiu na caraterização e implementação do sistema no que se refere à capacidade de expandir e comprimir impulsos laser para durações da ordem dos poucos ciclos ópticos (20 fs). Este tipo de sistemas laser encontra aplicação em campos como medicina, telecomunicações e maquinação, que requerem impulsos ultra-curtos (sub 100 fs) de alta energia.

O desafio residiu no estudo prévio, mas essencial para uma manipulação bem sucedida, de impulsos com largura de banda superior a 100 nm (com comprimento de onda central a 800 nm) quando amplificados de 4 ordens de grandeza (dos μJ a 20 mJ). Na realidade, o controlo, a manipulação e a caraterização dos fenómenos ópticos à escala de poucas dezenas de fs e com potências na ordem dos PW são extremamente complexos, devido aos complexos fenómenos que ocorrem como consequência da interacção radiação–matéria e a não-linearidade dos mesmos.

Com esse propósito foram caracterizados, de forma detalhada e rigorosa, os principais componentes dispersivos, incluindo a verificação da compressibilidade para larguras de banda menores que as finais de forma a garantir o bom desempenho destes elementos e prever a resposta para os impulsos pretendidos. A execução do trabalho obrigou a abordagens complementares como a caracterização do oscilador que alimenta a cadeia laser e à detecção e supressão de outras causas de dispersão.

Palavras-chave: Amplificação óptica paramétrica de impulsos dispersos; Impulsos laser ultra-curtos; Diagnósticos de impulsos; Compressão de impulsos; Dispersão óptica.

Contents

List of figures

List of tables

List of abbreviations

BBO	Beta barium borate (β-BaB_2O_4)
CEP	Carrier envelope phase
CPA	Chirped pulse amplification
CVBG	Chirped volume Bragg grating
DKDP	Potassium dideuterium phosphate (KD_2PO_4)
DOM	Disperse-O-Matic
FI	Faraday isolator
FPM	*femto*Pulse Master
FROG	Frequency-resolved optical gating
FTL	Fourier-transform limit
FWHM	Full-width at half the maximum intensity
GD	Group delay
GDD	Group delay dispersion
L2I	Laboratory for Intense Lasers
OPA	Optical parametric amplification
OPCPA	Optical parametric chirped pulse amplification
SHG	Second-harmonic generation
SHG-FROG	Second-harmonic generation frequency-resolved optical gating
TBWP	Time-bandwidth product
TGG	Terbium gallium garnet ($Tb_3Ga_5O_{12}$)
TOD	Third order dispersion
YAG	Yttrium aluminium garnet ($Y_3Al_5O_{12}$)

YCOB	Yttrium calcium oxyborate ($YCa_4O(BO_3)_3$)
WLC	White light continuum

List of symbols

A	Amplitude
B_n	Sellmeier coefficients
C_n	Sellmeier coefficients
c	Speed of light in vacuum
E	Electric field
G	Electric field of the gate pulse
g	Diffraction grating groove spacing
I	Intensity
$\boldsymbol{k}$	Wave vector
l	Optical path length
l_a	Optical path length between two prisms
l_{m}	Optical path length inside optical material
n	Refractive index
n_0	Refractive index at the central frequency or wavelength
$\mathrm{P}_{\mathrm{avg}}$	Average power
$\boldsymbol{R}$	Arbitrary vector
t	Time
γ	Incident angle
Δt	Full temporal width at half the maximum intensity
Δt_{AC}	Full autocorrelation temporal width at half the maximum intensity
$\Delta\lambda$	Spectral bandwidth (nm)
$\Delta\nu$	Frequency bandwidth (Hz)

δ	Phase lag
θ	Angle of diffraction/refraction
λ	Wavelength
λ_0	Central wavelength
ν	Frequency (Hz)
τ	Half temporal width at $1/e^2$ of the maximum intensity
ϕ	Phase
ϕ_a	Angular dispersion/phase
ϕ_m	Material dispersion/phase
ϕ_n	Phase terms of the phase Taylor expansion
ω	Angular frequency (rad)
ω_0	Central angular frequency (rad)

1

Introduction

More than 50 years of laser technology improvement – including the definition and implementation of important concepts as Q-switching in 1961[1], mode-locking in 1965[1] and chirped pulse amplification (CPA) in 1985[2] –, proved to be a milestone in science, enabling new areas of fundamental and applied physics and also finding new applications in chemistry, biology, medicine, telecommunications, industry, meteorology, security and many others. During this evolution, not only the increasing of laser pulse energy was boosted but also the decreasing of its duration assumed extreme values, leading to even higher and higher output peak power laser systems and to a new area of research: ultrafast science. In this new field ultrashort pulses of the order of few cycles are used to generate coherent harmonic radiation and attosecond pulses that can be used for example in visualization of biology and chemistry samples at atomic scales, and high-field physics.[3]

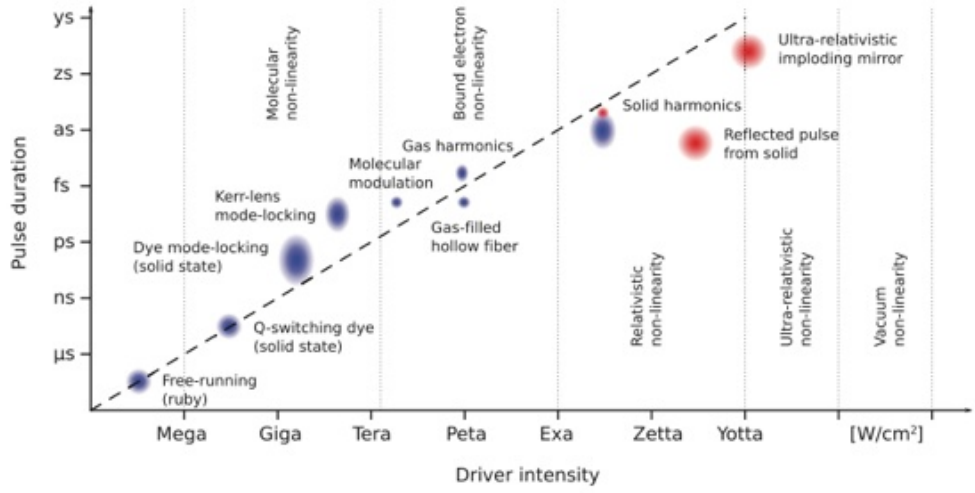

Figure 1.1: Progress in laser pulse intensity and duration.[4]

1.1 Chirped pulse amplification

Ultrashort pulses have a typical temporal width between 10^{-12} to 10^{-14} seconds allowing the generation of high peak optical powers even with relatively low pulse energies.[5] The generation of ultrashort pulses was possible with the improvement of mode-locking techniques and the Kerr-lensing effect. This led to the development of the Kerr-lens mode-locked Ti:sapphire laser,[6] a laser with a Ti:sapphire gain medium pumped by a solid state diode laser and a cavity that is preferentially made to lase in a pulsed mode rather than in a continuous wave mode. Due to a self-focusing process, fast self-amplitude modulation is achieved, generating mode-locked pulses and after dispersion compensation inside the cavity by a prism pair compressor, ultrashort pulses are released. As ultrashort pulses started to be commonly available there was an interest in finding new amplification techniques since laser amplifiers were restricted at that time to directly amplifying only longer input pulses. In 1985 one of the most important concepts for producing high-intensity, ultra-short laser pulses was introduced by Strickland and Mourou, based on pulse stretching and compression, overcoming the problem of nonlinear effects and optical damage – the chirped pulse amplification (CPA) technique. This concept consists in three steps: (1) stretching the pulse in time by passing it through a dispersive delay line, proportionally decreasing its peak intensity; (2) amplifying this chirped pulse in a conventional way; (3) compressing the pulse to its transform-limited duration increasing proportionally its peak intensity using another dispersive delay line that will compensate the induced chirp.[2] Stretching and compression can be achieved by optical elements such as bulk material, gratings, prisms, grisms and chirped-mirrors, enabling a dramatic increase in the maximum achievable peak intensity.[7]

1.2 Optical parametric chirped pulse amplification

Pulse stretching and compression are one of the most crucial stages in chirped pulse amplifiers, especially for few-cycle pulse amplifiers.[8] Although CPA systems have enabled the development of high-energy few-cycle pulses they can have several issues such as narrow spectral bandwidth, gain narrowing and amplified spontaneous emission, currently limiting them to the generation of PW-level pulses.[9] About 20 years ago an alternative technique for the generation of high-energy ultrashort pulses also based in the concept of stretching and compressing the optical pulses was introduced – optical parametric chirped pulse amplification (OPCPA).[7,10,11,12,13] Although recently introduced, OPCPA has already shown the potential to improve the laser pulse energy and duration, as well as repetition rate and pulse contrast, to values not previously achieved with conventional amplification.[13]

OPCPA results from a combination of CPA and another laser amplifier technology named optical parametric amplification (OPA).[14] The conjugation of CPA with a three-wave-mixing process (nonlinear optical phenomena) that occurs within an adequate nonlinear crystal – where a stronger, higher frequency input wave (pump pulse) trans-

fers energy to a weaker, lower frequency input wave (seed/signal pulse) generating also an auxiliary wave (idler pulse) due to energy and momentum conservation – that is OPA, is currently providing solutions to several of the CPA limitations, envisaging an output power up to the multipetawatt level.[14] Figure 1.1 represents the principle of three wave-mixing phenomena, described in terms of wave vectors and an energy diagram, showing the energy conservation during the process and the phase matching condition.

OPCPA has a number of advantages such as high gains per single pass, broad gain bandwidths, high quantum efficiency, low thermal deposition, reduced amplified spontaneous emission and high amplified signal beam quality with high contrast ratio.[11] All these highly desirable properties have led to a wide dissemination of OPCPA-based systems at high power laser laboratories around the world.

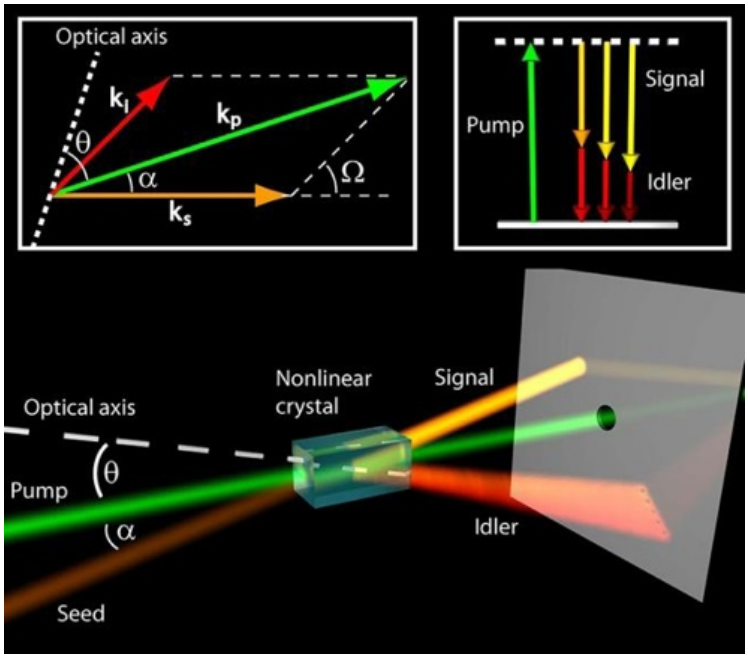

Figure 1.2: Schematic representation of the OPA main principle. The geometry represents a noncollinear interaction, where there is a small angle between the pump and signal beam directions.[5]

Two of the most important design choices for an OPCPA system are the pump technology and an appropriate nonlinear crystal, as they will determine the output characteristics of the system, such as average power, pulse energy and amplification bandwidth.[13] A common option is to use a CPA laser as a pump, and actually the highest pulse energies are generated by the use of flashlamp-pumped amplifiers,[15] while the highest average powers are allowed by the use of fiber-based pump technology.[16] However the disadvantages of these technologies are the limitation in terms of average power, in the case of the former, and the limitation in terms of pulse energies, in the case of the latter. Diode-pumped solid-state (DPSS) amplification[17] is in contrast a pump

technology that allows both high pulse energy and high repetition rates, thereby enabling high average power as well.

For the OPA part, there are also a number of possible crystal choices, with beta-barium borate (BBO)[18] and lithium triborate (LBO) being two of the most used non-linear crystals, thanks to their high non-linear coefficients and broad gain bandwidths. However, such choices are limited by the currently available crystal apertures, restricting their use to the pre-amplifier stages of high-energy laser systems. On the other hand, there are several examples that use large aperture potassium dideuterium phosphate (DKDP) crystals;[19] however its low non-linear coefficient and poor thermo-optic properties make it inadequate for high average power operation. The borate crystal yttrium calcium oxyborate (YCOB)[20] is a relatively recent and interesting alternative with a high nonlinear coefficient, large growth size capability and high damage threshold.[21]

1.3 Motivation of the thesis

A tabletop OPCPA system is being developed at the Laboratory for Intense Lasers (L2I)[21] to complement the laser amplifier technology currently available – a hybrid, flash-pumped Ti:sapphire/Nd:glass-based CPA.[22] The compactness and efficiency of this new system, together with a higher repetition rate, shorter pulses and lower pulse energies but comparable peak intensities, will allow for new experimental research of physical processes at the femtosecond scale in a much faster regime.

With the basic layout, delay lines and amplification stages of this OPCPA system already implemented, the compression and characterization of the output pulses are now some of the main concerns of the project. A stretching and compression setup had been proposed consisting in a SF11 glass block stretcher and a combination of prism pair and grating pair compressors, requiring a careful study and choice of the optimum parameters for the optical devices to efficiently stretch and compress the signal pulses before and after the two YCOB crystals before applying them on the OPCPA.

In fact, the last part of the OPCPA system and the main concern of this project is the stretching and compression of the amplified pulses, since for a final pulse with a duration of just a few tens of femtoseconds higher dispersion orders have to be compensated for compression close to the Fourier transform limit (FTL). Because we are dealing with very broadband spectra, even a small amount of these dispersion orders will cause a relevant increase in the pulse duration.

1.4 Thesis work outline

In order to efficiently design and implement the stretching and compression stages of the OPCPA system, with its optical elements, the current thesis work is organized in

around the following three major goals, which will be presented and discussed along the next chapters:

(1) to perform numerical simulations for different parameters of the gratings and prisms configuration;

(2) to characterize experimentally the dispersion caused by the most relevant optical components to be used in the setup with the available bandwidth (~20 nm) coming directly from the oscillator;

(3) to compare the experimental results with the predicted ones and extrapolate them to wavelength intended for OPCPA operation (650-1000 nm). With this data we can evaluate whether the design and dispersive optical media used are appropriate for the compression of the OPCPA output pulses down to 20 fs duration.

After this short introduction (Chap. 1), the thesis continues with the theory underlying pulse stretching and compression (Chap. 2), which includes the concepts of material and angular dispersion, Taylor expansion of the spectral phase up to several orders, as well as their influence on the temporal profile of the pulse. The optical materials that are proposed to generate and compensate the dispersion of the optical pulses are also introduced in Chapter 2.

Chapter 3 is devoted to the characterization of ultrashort pulses, that is to the theory of ultrashort pulse measurement and a description of the measuring diagnostics used in the experimental work. The characterization of the pulses to be stretched and compressed is presented at the end of this chapter.

In Chapter 4 the theoretical study and experimental characterization of the stretching and compression optical media are reported. The experimental data is followed by an analysis and discussion.

Chapter 5, although short, addresses the important issue of the extrapolation to the operating bandwidth of the OPCPA system. Based on the previous results we analyse and discuss the expected performance and suitability at the effective projected parameters.

Finally, in Chapter 6 we perform an overall evaluation of the results achieved, and discuss future work directions.

2

Pulse Stretching and Compression

Pulse stretching and compression are only made possible by the introduction of dispersive optical setups of opposite signs. Since ultrashort pulses, characterized by their short durations, have large frequency bandwidths the concept is based on generating a controllable delay for each frequency and so expanding the pulse in time; also, removing the same delay we can then have a pulse that is compressed in time. The insertion of this delay can be achieved by propagating the optical pulses through an optical material or inside dispersive optical devices such as grating pairs or prism pairs. The resulting stretched pulse also becomes chirped, with a sign that depends on the overall dispersion sign.

2.1 Dispersion

The electric field in the temporal domain $E(t)$ of an ultrashort optical pulse can be defined as:[5,23,24]

$$E(t) = A(t)\cos(\phi + \omega t) \tag{2.1}$$

where $A(t)$ is the temporal amplitude or envelope function, ϕ is the temporal phase and ω is the carrier circular or angular frequency. However, since its electric field in the temporal domain $E(t)$ is difficult to access and we are dealing with dispersion, the spectral/frequency domain $\tilde{E}(\omega)$ is preferentially studied, and we can relate the two by means of a Fourier transform:

$$E(t) = \frac{1}{2\pi}\int_{-\infty}^{\infty} \tilde{E}(\omega)e^{i\omega t}d\omega \tag{2.2}$$

Similarly to the temporal domain in Eq. (2.1), the inverse Fourier transform can be defined by:

$$\tilde{E}(\omega) = A(\omega)e^{-i\phi(\omega)} \tag{2.3}$$

where the spectral amplitude $A(\omega)$ and the spectral phase $\phi(\omega)$ are parameters that we can measure and control, and so influence the temporal properties of the optical pulse. One common approach for the description in the spectral domain consists in writing the spectral phase $\phi(\omega)$ as a Taylor series around the central frequency ω_0:

$$\phi(\omega) = \phi_0(\omega_0) + \phi_1(\omega - \omega_0) + \frac{1}{2}\phi_2(\omega - \omega_0)^2 + \frac{1}{6}\phi_3(\omega - \omega_0)^3 + \ldots + \frac{1}{n!}\phi_n(\omega - \omega_0)^n \qquad (2.4)$$

with $\phi_n = \left.\frac{d^n\phi(\omega)}{d\omega^n}\right|_{\omega_0}$.

Often, the first terms of Eq. (2.4) are the most important and needed to control the pulse temporal width and shape with each of them playing a different dispersion role, as follows:

- ϕ_0 is the phase between the envelope and carrier frequency, known as the absolute phase or carrier envelope phase (CEP);
- ϕ_1 is the linear phase or group delay (GD), and it represents a constant time shift or time delay between the pulse and an origin time reference. This is a simple translation in the time domain, causing no changes in the shape or duration of the pulse. Thus, a plus sign will only mean that the pulse arrived after the reference time and, similarly, a minus sign will stand for a pulse that arrived before;
- ϕ_2 is the quadratic phase or group delay dispersion (GDD), responsible for temporally stretching the pulse. It corresponds to a delay that varies linearly with the frequency and thus introduces a linear chirp on the pulse (Figure 2.1). For normal dispersion (such as that caused by optical glasses) longer wavelengths travel faster than shorter ones, and this term is positive; otherwise, a negative term represents the case where the "blue" spectral components travel faster than the "red" ones, as happens for anomalous dispersion;
- ϕ_3 is the cubic phase or third order dispersion (TOD). It is responsible for introducing pre and post-pulses in the temporal domain. Both higher and lower frequencies will arrive after (or before, depending on the sign of the TOD) the central frequencies, causing beats in the temporal intensity profile (Figure 2.1). This term and the previous one are the most important parameters for the present work, since the simultaneous cancellation of GDD and TOD is the main requirement to obtain ultrashort, few-cycle pulses;
- finally, ϕ_n represents the generic higher order phase terms, which are difficult to compensate, and does not have to be taken into account for the type of pulses we intend to obtain.

2.2 Pulse duration after dispersion

If we assume that the temporal shape of the optical pulse has a Gaussian profile we can define the temporal intensity function $I(t)$ of the beam as:[22,25]

$$I(t) = I_0 e^{-4\ln 2\left(\frac{t}{\Delta t}\right)^2} \tag{2.5}$$

where I_0 is the amplitude of the intensity, Δt is the full-width at half the maximum (FWHM) temporal intensity profile. It is useful to relate this quantity to that obtained from the half-width at $1/e^2$ of the maximum temporal intensity profile τ, once τ is also a common value used for the characterization of the optical pulses. Thus, knowing that:

$$\Delta t = \tau\sqrt{2\ln 2} \tag{2.6}$$

we obtain for the temporal intensity, similarly to Eq. (2.5), the following:

$$I(t) = I_0 e^{-2\left(\frac{t}{\tau}\right)^2} \tag{2.7}$$

Other consideration is that working with this type of phenomena requires the determination of the Fourier-transform limit (FTL) of the optical pulse, which is defined as the shortest temporal duration possible for a given spectral width, corresponding to a flat spectral phase (a particular case where $\phi(\omega) = 0$ is shown in Figure 2.1).[23] Thus, given an optical pulse with a known duration and spectral width, by calculating its FTL it is possible to estimate how far we are from a thoroughly compressed pulse. For a Gaussian shaped pulse with a bandwidth $\Delta\nu$ or $\Delta\lambda$ we can determine the shortest pulse duration Δt by using the definition of the time-bandwidth product (*TBWP*):

$$TBWP = \Delta t\Delta\nu = \frac{c}{\lambda^2}\Delta t\Delta\lambda = 0.441 \tag{2.8}$$

where c is the speed of light (note that this relation is given in terms of the frequency ν or wavelength λ instead of the angular frequency ω, since those parameters are most commonly used).

Although we will not use it in this work, it is important to mention another common optical pulse shape – the hyperbolic secant squared function, in which case we should consider the TBWP as the following:

$$TBWP = \Delta t\Delta\nu = \frac{c}{\lambda^2}\Delta t\Delta\lambda = 0.315 \tag{2.9}$$

Ultrashort pulses characterized by their short duration have consequently large spectral bandwidths, this is, a coherent superposition of a broad range of frequencies[26] meaning that they can be easily broadened in time with the insertion of just a small spectral phase quantity ϕ_2 but that this same amount must be carefully compensated. Note that, for example, if we have a pulse with a central wavelength λ = 800 nm, from Eq. (2.8), a 20 fs pulse duration requires a bandwidth of approximately 50 nm what is a considerable large bandwidth when compared with amplified pulse bandwidths delivered in traditional high-gain amplification processes.[27]

The relation between the introduced GDD (i.e. ϕ_2) in an optical pulse with an initial FTL pulse duration Δt_{in} and the output duration of the linearly chirped pulse Δt_{out} is given by:[24]

$$\Delta t_{out} = \Delta t_{in}\sqrt{1+\left(4\ln 2\frac{\phi_2}{\Delta t_{in}^2}\right)^2} \tag{2.10}$$

(note that this relation is valid for a Gaussian shaped pulse with the pulse durations measured at the FWHM). The equivalent relation in terms of the half-width at $1/e^2$ of the maximum intensity τ is defined as:

$$\tau_{out} = \tau_{in}\sqrt{1+\left(2\frac{\phi_2}{\tau_{in}^2}\right)^2} \tag{2.11}$$

where τ_{in} is the initial half-width at $1/e^2$ of the maximum intensity FTL pulse duration and τ_{out} is the correspondent output duration.

Furthermore, as we already said, we must consider the introduced TOD value ϕ_3 and, similarly to Eqs. (2.10) and (2.11), we can relate the output pulse duration Δt_{out} with the initial FWHM FTL pulse duration Δt_{in} and its TOD value ϕ_3, as well as, the output half-width at $1/e^2$ of the maximum intensity pulse duration τ_{out} with its initial FTL pulse duration τ_{in} and TOD value ϕ_3:[24]

$$\Delta t_{out} = \Delta t_{in}\sqrt{1+\ln 2\left(4\ln 2\frac{\phi_3}{\Delta t_{in}^3}\right)^2} \tag{2.12}$$

$$\tau_{out} = \tau_{in}\sqrt{1+\frac{1}{2}\left(2\frac{\phi_3}{\tau_{in}^3}\right)^2} \tag{2.13}$$

From Eqs. (2.10) and (2.12) we can write the total duration of the output pulse at the FWHM considering both orders, and analogously from Eqs (2.11) and (2.13) we will have the total output duration at the half-width at $1/e^2$ of the maximum intensity:

$$\Delta t_{out} = \Delta t_{in}\sqrt{1+\left(4\ln 2\frac{\phi_2}{\Delta t_{in}^2}\right)^2+\ln 2\left(4\ln 2\frac{\phi_3}{\Delta t_{in}^3}\right)^2} \tag{2.14}$$

$$\tau_{out} = \tau_{in}\sqrt{1+\left(2\frac{\phi_2}{\tau_{in}^2}\right)^2+\frac{1}{2}\left(2\frac{\phi_3}{\tau_{in}^3}\right)^2} \tag{2.15}$$

The required dispersion coefficients ϕ_2 and ϕ_3 to obtain the intended output durations can be generated by material dispersion, as the refractive index depends of frequency/wavelength, or through angular dispersion, this is, either from refraction or diffraction phenomena, as we will explain in the next parts of this chapter.

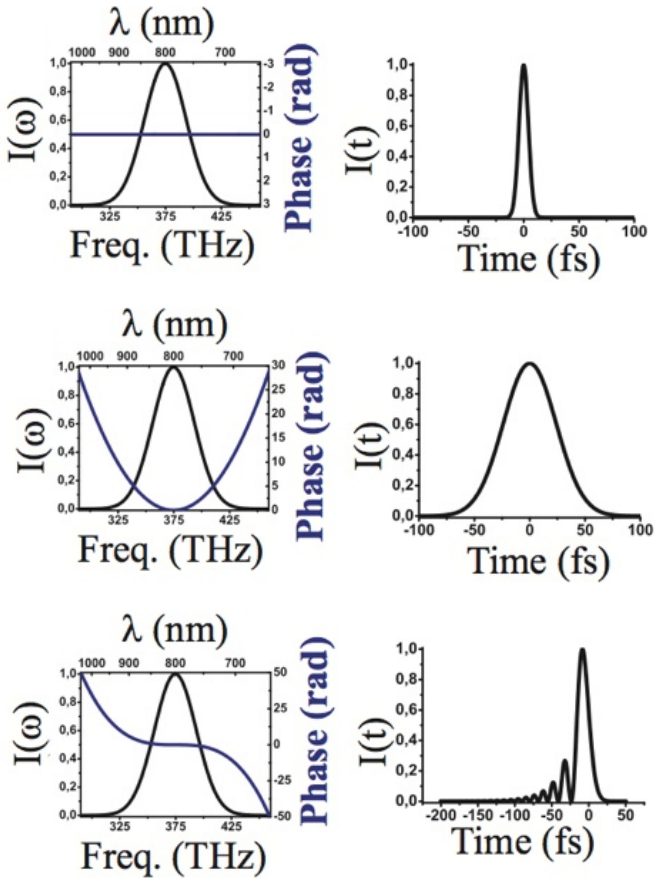

Figure 2.1: Examples for the introduction of quadratic and cubic phases on the pulse. Upper box: FTL pulse which corresponds to a zero spectral phase; middle box: insertion of a positive quadratic phase, broadening the pulse in time; lower box: insertion of a negative cubic phase leading to a stronger pulse preceded by an increasing pulse sequence.[23]

2.3 Group delay dispersion and third order dispersion

The spectral phase $\phi(\omega)$ induced by a generic stretcher or compressor device can be defined as:[28]

$$\phi(\omega) = \vec{k}(\omega) \cdot \vec{R} = |k(\omega)||R|\cos\theta \tag{2.16}$$

where $\boldsymbol{k}$ is the wave vector of the frequency ω whose modulus is given by:

$$k(\omega) = \frac{\omega n}{c} \tag{2.17}$$

with n being the refractive index of the medium and c the speed of light; $\boldsymbol{R}$ is an arbitrary vector that extends throughout the system and θ is the angle between these two vectors. Since the wave vector depends on frequency, for each spectral component it may have a different length and direction. The difference between the projections of these different wave vectors on the arbitrary vector will give us the phase lag (Figure 2.2). Replacing Eq. (2.17) into Eq. (2.16) we have:

$$\phi(\omega) = \frac{l}{c}\omega n(\omega)\cos[\theta(\omega)] \tag{2.18}$$

where $l \equiv R$ is the length travelled by the central frequency ω_0 of the optical pulse through the dispersive line. Note that the refractive index n and the angle θ are frequency-dependent.

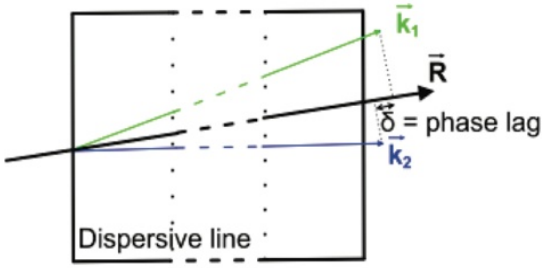

Figure 2.2: Schematic representation of the formalism used to calculate the spectral phase. The geometry represents two different wave vectors $\boldsymbol{k}_1$ and $\boldsymbol{k}_2$, their projection over an arbitrary vector $\boldsymbol{R}$, and the optical path difference between them (this is, the phase lag δ).[28]

Note that we had previously written the spectral phase $\phi(\omega)$ in terms of a Taylor expansion in Eq. (2.4). By differentiating Eq. (2.18) we may calculate each of the expansion coefficients. Differentiating this relation once around the central frequency ω_0 and expressing it in terms of wavelength λ instead of frequency ω, since it is simpler and more useful to work with, we obtain the linear spectral phase term:

$$\phi_1 = \left.\frac{d\phi(\lambda)}{d\lambda}\right|_{\lambda_0} = \frac{l}{c}\left[n_0 - \lambda_0 \left.\frac{dn(\lambda)}{d\lambda}\right|_{\lambda_0}\right] \tag{2.19}$$

where n_0 is the index of refraction of the material crossed by the optical pulse with a central wavelength λ_0 that can be determined from the Sellmeier equation (see Sec. 2.3.1).

Similarly, we obtain the second and third derivates of Eq. (2.18) in terms of the wavelength λ. As we have in both of these cases not only the contribution from the material properties but also an angular dependence, we can separate the two different contributions and write the quadratic phase ϕ_2 and the cubic phase ϕ_3, this is GDD and TOD terms, as follows:

$$\phi_2 = \left.\frac{d^2\phi(\lambda)}{d\lambda^2}\right|_{\lambda_0} = \overbrace{\frac{\lambda_0^3 l}{2\pi c^2}\left.\frac{d^2 n(\lambda)}{d\lambda^2}\right|_{\lambda_0}}^{\phi_{2m}} - \overbrace{\frac{\lambda_0^3 n_0 l}{2\pi c^2}\left[\left.\frac{d\theta(\lambda)}{d\lambda}\right|_{\lambda_0}\right]^2}^{\phi_{2a}} \tag{2.20}$$

$$\phi_3 = \left.\frac{d^3\phi(\lambda)}{d\lambda^3}\right|_{\lambda_0} \tag{2.21}$$

$$= \overbrace{-\frac{\lambda_0^4 l}{4\pi^2 c^3}\left[3\frac{d^2 n(\lambda)}{d\lambda^2}\bigg|_{\lambda_0} + \lambda_0 \frac{d^3 n(\lambda)}{d\lambda^3}\bigg|_{\lambda_0}\right]}^{\phi_{3m}}$$

$$+ \overbrace{\frac{3\lambda_0^4 n_0 l}{4\pi^2 c^3}\frac{d\theta(\lambda)}{d\lambda}\bigg|_{\lambda_0}\left[\frac{d\theta(\lambda)}{d\lambda}\bigg|_{\lambda_0} + \lambda_0 \frac{d^2\theta(\lambda)}{d\lambda^2}\bigg|_{\lambda_0}\right]}^{\phi_{3a}}$$

where we can clearly see that the first term of the right hand side in each equation corresponds to the material dispersion ϕ_m and the second part is the angular dispersion ϕ_a.

These are general equations for the GDD and TOD, i.e. Eqs. (2.20) and (2.21), can be particularized for the different optical devices discussed in this work as we will demonstrate in the next sections.

2.3.1 Transparent media

When a transform-limited optical pulse travels a distance l inside a material with index of refraction $n(\lambda)$, either gas, liquid or solid, it will undergo a temporal broadening since different wavelengths experience different frequency-dependent time delays. For normal incidence into the medium there is no angular contribution ($d\theta/d\lambda = 0$) and we can reduce GDD and TOD, defined in Eqs. (2.20) and (2.21) to their material dispersion terms ϕ_{2m} and ϕ_{3m}:[24]

$$\phi_2 = \phi_{2m} = \frac{\lambda_0^3 l}{2\pi c^2}\frac{d^2 n(\lambda)}{d\lambda^2}\bigg|_{\lambda_0} \tag{2.22}$$

$$\phi_3 = \phi_{3m} = -\frac{\lambda_0^4 l}{4\pi^2 c^3}\left[3\frac{d^2 n(\lambda)}{d\lambda^2}\bigg|_{\lambda_0} + \lambda_0 \frac{d^3 n(\lambda)}{d\lambda^3}\bigg|_{\lambda_0}\right] \tag{2.23}$$

The Sellmeier equation is an empirical relationship that allows us to compute the wavelength dependence of the refractive index for a transparent medium, and can be written as:

$$n^2(\lambda) = 1 + \frac{B_1\lambda^2}{\lambda^2 - C_1} + \frac{B_2\lambda^2}{\lambda^2 - C_2} + \frac{B_3\lambda^2}{\lambda^2 - C_3} \tag{2.24}$$

where $B_{1,2,3}$ and $C_{1,2,3}$ are the experimentally determined Sellmeier coefficients, which are usually available from the supplier of the material.

In this work a 12.5 cm long block of SF11 glass is used and characterized to introduce positive GDD and TOD as a stretcher. Replacing Sellmeier coefficients[29] into Eq. (2.24) we can estimate the dispersion caused by 1 mm of SF11 for any central wavelength from Eqs. (2.22) and (2.23). Since in this work we are only interested in laser pulses at 900 nm and 1030 nm central wavelengths, both dispersion coefficient values are shown in

Table 2.1. Note that the dispersion caused by the same amount of glass is higher for lower wavelengths.

Among common optical materials, SF11 is one of the highly dispersive glasses (see Tables 2.1 and 2.2). In fact, if we compare for example the dispersion coefficients of fused silica and SF11 we can see that they are several times large for the latter. For this reason SF11 is most commonly used to introduce dispersion as a simple glass block or in a prism configuration (see Sec. 2.3.3), while fused silica is preferably used for optical windows such that short pulses may pass without suffering dispersion effects, i.e., fused silica is chosen as it introduces a minimal dispersion amount. However, when computing the total dispersion terms for a stretcher-compressor assembly delivering an output pulse of a few tenths of femtoseconds, it is important to take into account that although minimal when compared with the contribution of SF11 glass, material dispersion caused by other optical materials along the system (such as crystals, lenses, polarizers, waveplates, filters and of other optical components) must be taken into account. Note that for common materials we have both GDD and TOD with a positive sign, meaning a normal dispersion and positive TOD, and that each contribution will be added to the others.

Table 2.1: Calculated dispersion coefficients for SF11 glass and respective TOD/GDD ratios.

λ_0 (nm)	GDD/mm (fs^2/mm)	TOD/mm (fs^3/mm)	TOD/GDD (fs)
900	157.2	119.9	0.76
1030	125.7	119.5	0.95

Table 2.2: Dispersion coefficients for different materials at 900 nm wavelength and respective TOD/GDD ratios.

Material	GDD/mm (fs^2/mm)	TOD/mm (fs^3/mm)	TOD/GDD (fs)
Fused Silica	28.5	31.9	1.12
BK7	35.6	36.2	1.02
Sapphire	46.3	48.1	1.04
KDP	16.3	60.6	3.72
Calcite	61.2	35.1	0.57
Air	0.02	0.001	0.05

2.3.2 Transmission grating pair

A grating pair arrangement is an angular highly dispersive optical device classically used to compensate large amounts of dispersion.[30] Its angular dispersion is caused by diffraction and thus the angle θ for which the wavelength λ is diffracted can be expressed as:[28]

$$\sin[\theta(\lambda)] = \frac{m\lambda}{g} - \sin\gamma \tag{2.25}$$

where γ is the incident angle, m is the order of diffraction and g is the space between the grooves of the grating.

Since now the dispersion is exclusively angular, because the optical path l is performed in the air ($n(\lambda) \approx 1$), we can then remove the material contribution in Eqs. (2.20) and (2.21) and replace Eq. (2.25) into them:

$$\phi_2 = \phi_{2a} = -\frac{\lambda_0^3 l}{2\pi c^2}\left(\frac{m}{g\cos[\theta(\lambda)]}\right)^2 \tag{2.26}$$

$$\phi_3 = \phi_{3a} = \frac{3\lambda_0^4 l}{4\pi^2 c^3}\left(\frac{m}{g\cos[\theta(\lambda)]}\right)^2\left(1 + \frac{\lambda_0 m}{g}\frac{\sin[\theta(\lambda)]}{\cos^2[\theta(\lambda)]}\right) \tag{2.27}$$

Note that for convenience, we may also use the perpendicular distance between gratings L_g instead of the optical path l which can be related simply by:

$$L_g = l\cos[\theta(\lambda)] \tag{2.28}$$

Although the most common optical diffraction gratings are of the reflecting type, transmission gratings are also popular and used for the same purpose, as it happens in our case. Both types can be used in a typical compact pair configuration, where the two identical plane ruled gratings are placed parallel to each other and followed by a retroreflector mirror. Mainly, the optical pulse reaches the first grating with a chosen incident angle γ, normally closed to the Littrow configuration where the incident angle corresponds to the highest efficiency of the grating,[31] and its different component wavelengths are diffracted according to Eq. (2.25) into various orders. The second grating is positioned in the direction of the high efficiency first order, and once the beam reaches this second grating it emerges collimated along the same direction as the incident beam on the first grating. The beam is then reflected backwards, into the same grating pair, in order to remove the spatial chirp. Since longer wavelengths had to travel a longer optical pathlength than shorter wavelengths, through all this setup, the beam will be temporally stretched and anomalously dispersed (Figure 2.3), resulting in a negative GDD. Note that the TOD sign is the opposite of the GDD term.

It is also important to note that for the configurations described above we must multiply both Eqs. (2.26) and (2.27) by a factor of 2 when computing the total amount of GDD and TOD inserted by the whole device, in order to account for the double pass for each dispersion order.

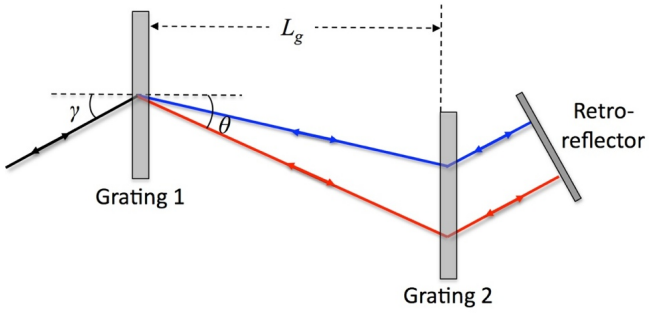

Figure 2.3: Schematic diagram of a transmission grating pair. Angular dispersion causes the redder components of the pulse to travel a longer distance than the bluer components, resulting in a negative chirp.[9]

In this work we use a 300 grooves/mm blazed transmission grating pair with a blaze angle of 31.7° with peak efficiency around 800 nm.[31] The main reasons for using transmission grating pair are a lower sensibility to the alignments and that they are easy to manage while using a compact configuration for large bandwidths. The number of grooves was chosen since sufficient GDD can be introduced this way in a compact configuration while working closer to the Littrow configuration and at the same time introducing less TOD than a grating with a higher number of grooves/mm. In fact, dispersion depends mainly on four parameters: groove density, angle of incidence, distance between gratings and wavelength; and this variation differs for GDD and TOD. Higher density grooves compensate large amounts of GDD in a very short distance with cost of a higher TOD/GDD ratio and the greater the wavelength used the higher will be this ratio. However lower density grooves not only worsen the compactness of the compressor but also its efficiency. Thus, the choice of the adequate grating must result from a compromise of both considerations. After choosing the grating the parameters that can be changed will be the distance that will allow for a large tune of the dispersion and the variation of the angle that should be closer to the Littrow configuration and will allow for a fine tune. Variation of GDD and TOD with the distance L_g for two different wavelengths, 900 nm and 1030 nm, generated by gratings with 15, 300 and 600 groves/mm at a fixed angle corresponding to Littrow configuration can be compared in Figure 2.4. Associated to each grating is the TOD/GDD ratio for the two wavelengths at the Littrow angle. The variation of the dispersion with the angle for a fixed distance at 900 nm can also be found in Figure 2.4.

The main disadvantages of using this setup are not only the insertion of a significant amount of positive TOD but also the wavelength-dependent transmission efficiency – i.e. transmission has not a constant behavior for all the wavelengths leading, for example, to spectral narrowing –, and the low efficiency after passing twice through each grating.[9]

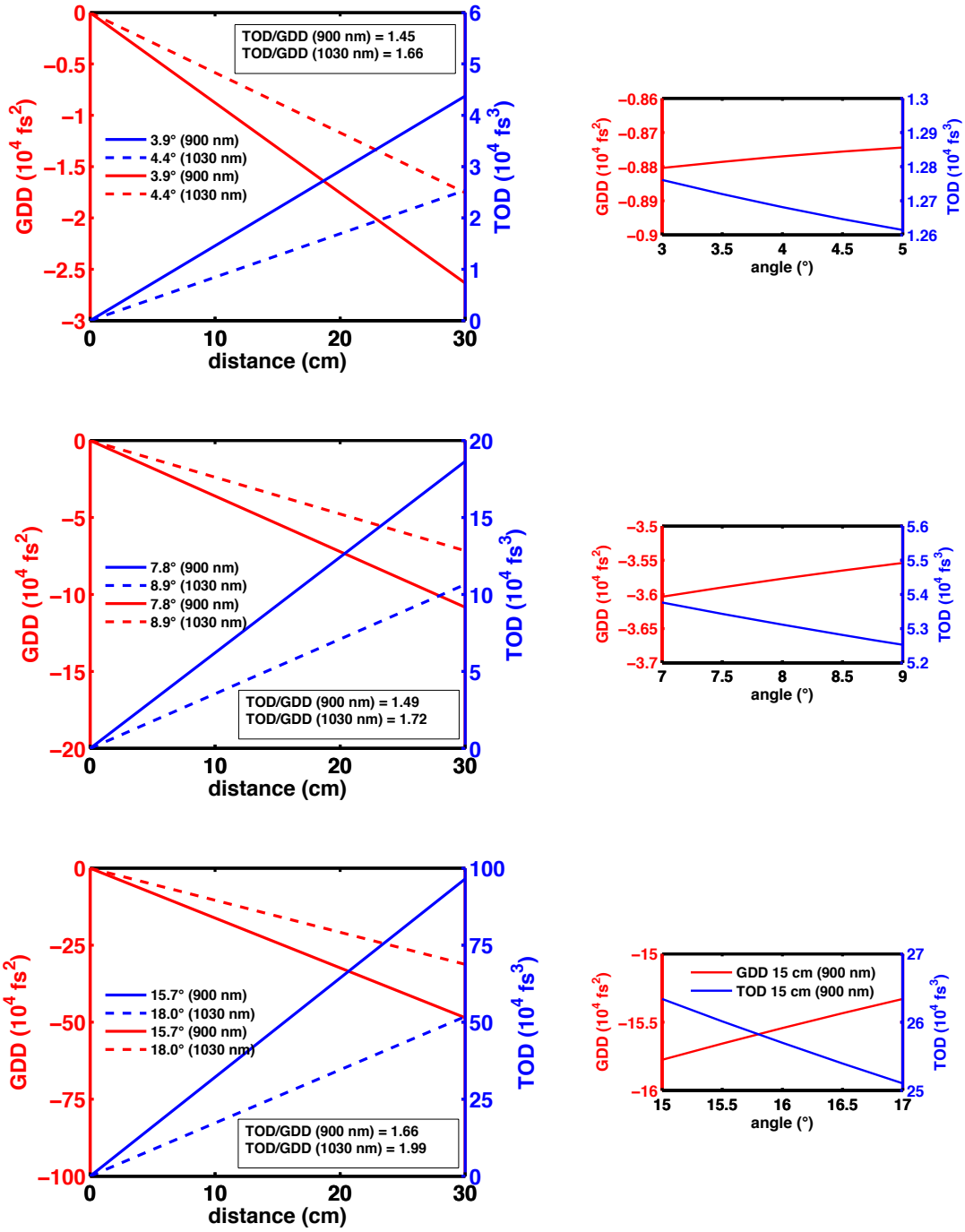

Figure 2.4: Variation of GDD (blue lines) and TOD (red lines) generated by 150 g/mm (top), 300 g/mm (middle) and 600 g/mm (bottom) grating pair compressors at 900 nm (solid line) and 1030 nm (dashed line) for fixed Littrow angles at different perpendicular distances between gratings (left) and for a fixed distance of 15 cm at different near Littrow incident angles (right). TOD/GDD ratio for is added to the different gratings.

2.3.3 Brewster prism pair

Prism pairs are also commonly used to remove or introduce dispersion in optical pulses.[32] Since their angular dispersion is due to refraction phenomena, by using Snell's Law the refracted angle θ at the interface between the two different media of refractive indexes n_1 and n_2, for a beam with an incident angle γ can be expressed as:[28]

$$\sin[\theta(\lambda)] = \frac{n_1(\lambda)}{n_2(\lambda)}\sin\gamma \tag{2.29}$$

Still, the laser beam will travel inside the prisms, meaning that it will cross a significant amount of material. Therefore, the optical pulse will undergo temporal spreading not only from angular dispersion but also from material dispersion. Thus, considering l_m the distance that the central wavelength of the optical pulse travels inside the material and l_a the optical path of the central wavelength performed between the two prisms due to angular dispersion we have:

$$\phi_2 = \phi_{2m} + \phi_{2a} = \frac{\lambda_0^3 l_m}{2\pi c^2}\left.\frac{d^2 n(\lambda)}{d\lambda^2}\right|_{\lambda_0} - \frac{2\lambda_0^3 l_a}{\pi c^2}\left[\left.\frac{dn(\lambda)}{d\lambda}\right|_{\lambda_0}\right]^2 \tag{2.30}$$

$$\begin{aligned}\phi_3 = \phi_{3m} + \phi_{3a} = &-\frac{\lambda_0^4 l_m}{4\pi^2 c^3}\left[3\left.\frac{d^2 n(\lambda)}{d\lambda^2}\right|_{\lambda_0} + \lambda_0\left.\frac{d^3 n(\lambda)}{d\lambda^3}\right|_{\lambda_0}\right] \\ &-\frac{3\lambda_0^4 l_a}{\pi^2 c^3}\left.\frac{dn(\lambda)}{d\lambda}\right|_{\lambda_0}\left[\left.\frac{dn(\lambda)}{d\lambda}\right|_{\lambda_0} + \lambda_0\left.\frac{d^2 n(\lambda)}{d\lambda^2}\right|_{\lambda_0}\right]\end{aligned} \tag{2.31}$$

A typical prism pair arrangement (such as the one used in this work) consists in a similar setup to the above described grating pair: two prisms are placed parallel with their apex angles opposite to each other, such that the first one will introduce refraction and the second will collimate the spatially dispersed beam. A retroreflector mirror will send the pulse back into both prisms, coming out temporally broadened but with no spatial chirp (Figure 2.5). Although, in this case, the "blue" components travel a longer distance in the air than the "red" components, suggesting a normal dispersion, the pulse will end negatively dispersed as the latter cross a thicker amount of material in the second prism than the former, making it an optical device less dispersive than the previous one.[9] Also note that for the GDD the material contribution has an opposite sign to the angular contribution, and that by inserting more or less material into the device – i.e. by translating the second prism –, we can tune/control the amount of dispersion that we want to insert or compensate, making prism pairs ideal for dealing with smaller amounts of dispersion.[9] An important observation too is that unlike the dispersion induced by the grating pair device, in the prism pair, both GDD and TOD will have negative signs provided the material contribution is lower than the angular, which is the most common situation.

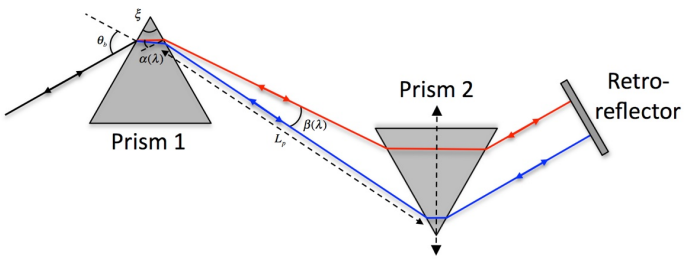

Figure 2.5: Schematic diagram of a prism pair. In this case, angular dispersion and material dispersion inside the second prism can be tuned to provide desired amounts of GDD and TOD.[9]

Once again, for the same reason as in Sec. 2.3.2, we must multiply the GDD and TOD in Eqs. (2.30) and (2.31) by a factor of 2 (note that the material distance l_m is the sum of the lengths travelled inside the first prism and inside the second one in a single pass).

In this work we use a 59° Brewster prism pair made of the same material as the glass block, SF11. The choice of SF11 is due to its high dispersion already explained before (c.f. Sec 2.3.1) and its 59° apex angle corresponds to the angle that allows for both higher transmission, which happens while using a Brewster incident angle, and a minimum deviation angle, which occurs when the beam travels parallel to the base of the prism.[33] Since prisms are intended to compensate the TOD it is important to have not only a high TOD/GDD ratio (requiring less distance in the prisms to compensate the TOD) but the main requirement is that they should cancel the TOD amount in a minimum apex-to-apex distance configuration, i.e. using a compact setup. If we compare, for example, SF11 Brewster prism pair with a BK7 Brewster prism pair (apex angle = 67°) we will find that the latter has a higher TOD/GDD ratio and will require much longer distances between prisms to compensate the same amount of dispersion (Figure 2.6). As the GDD and TOD are wavelength-dependent the TOD/GDD ratio will also be different for different wavelengths being higher for shorter ones (Figure 2.6). In addition to the angular dispersion caused by the material, the wavelength-dependence and the linear variation with the apex-to-apex distance, variation of the dispersion with the insertion of material in the second prism for a fixed apex-to-apex distance at 900 nm can be also found in Figure 2.6 for both compressors.

Thus, the main disadvantage of this setup is the need of longer distances for the same amount of dispersion between the prisms, as well as larger prisms. (Note that these examples were done for the same distances as gratings in Figure 2.4 and that the correspondent amounts of GDD and TOD introduced are much shorter even for the higher dispersive prism pair.) And although making more passes in the prism pair could reduce its size it will have a cost in its efficiency.[9]

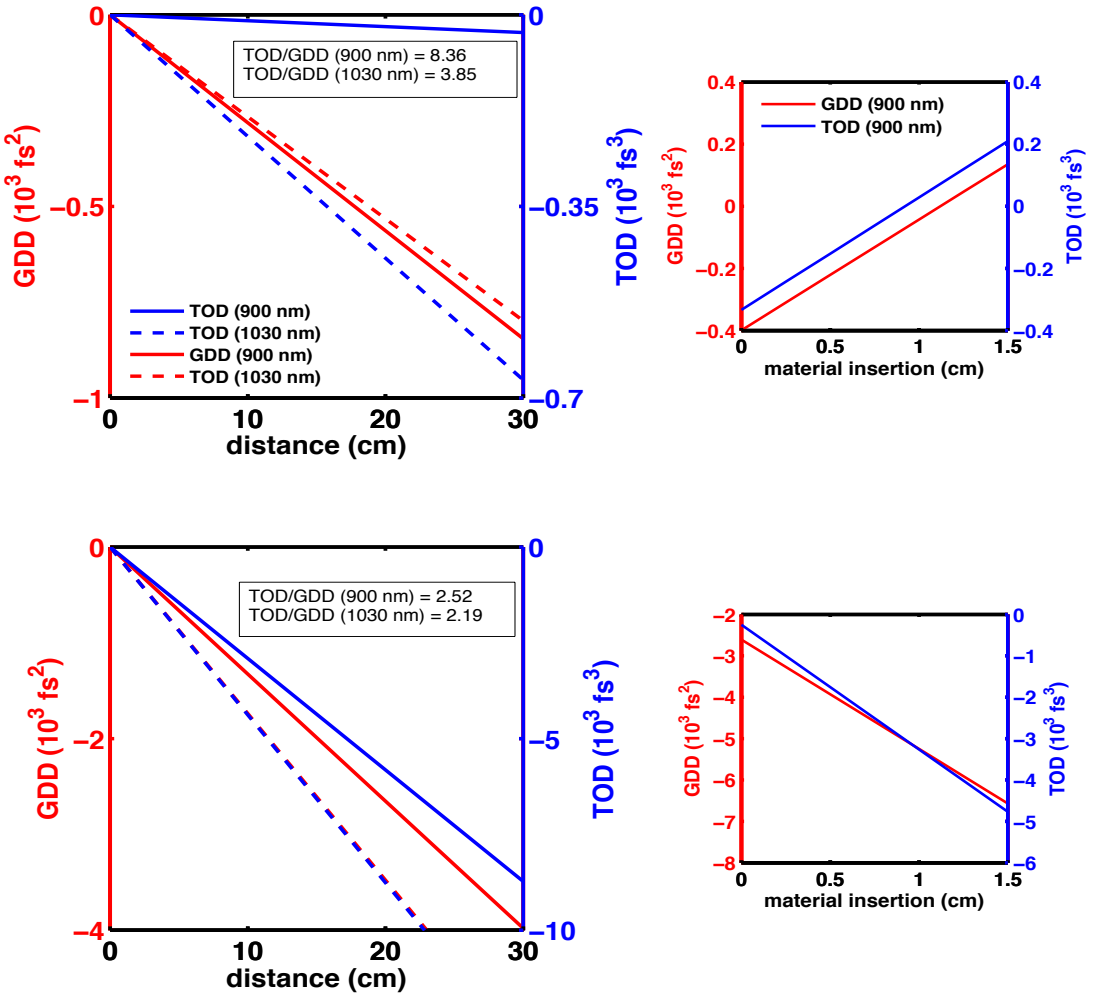

Figure 2.6: Variation of GDD (blue lines) and TOD (red lines) generated by BK7 (top) and a SF11 (bottom) prism pair compressors at 900 nm (solid line) and 1030 nm (dashed line) for fixed apex angles (59° for the first compressor and 67° for the latter) at different apex-to-apex distances between prisms (left) and for a fixed distance of 15 cm with different material insertion length (right). TOD/GDD ratio is added to the different gratings.

2.3.4 Chirped mirror pair

Chirped mirror pairs allow making an ultrafine tune/control of the GDD and they are frequently used to support compression of ultrashort pulses with few optical cycles.[34] The dispersion management is made possible thanks to successive dielectric layers, each reflecting a different wavelength. These layers are made of two different transparent materials, one with a higher index of refraction n_H and the other with a lower refractive index n_L, typically titanium dioxide (TiO_2) and silicon dioxide (SiO_2) respectively, put together in an alternating sequence.[35] The thickness of each layer is commonly one quarter of the wavelength for which the layer is design, starting with the larger ones closer to the substrate and then decreasing thickness gradually into the top. Thus, as any spectral component is reflected in a different layer and so in a different depth of the mirror, every wavelength will experience a different optical path thereby introducing a chirp on the

optical pulse. As longer wavelengths go deeper into the mirror and shorter ones are reflected at the surface layers this leads to a negative GDD (Figure 2.7). Chirped mirrors with an opposite configuration may also be found, thus leading to a positive GDD.

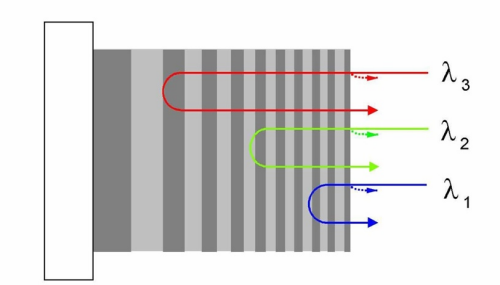

Figure 2.7: Schematic representation of the operation principle of a chirped mirror. Longer wavelengths will experience longer optical paths since they penetrate deeper into the mirror structure thus resulting in anomalous dispersion of the pulse.[34]

Typically chirped mirrors are used in pairs, that is, two chirped mirrors are placed parallel to each other enabling bouncing back and forth the laser pulse.[36] Each bounce on a mirror will introduce a certain quantity of dispersion being the number of passages as many as needed to introduce or compensate the intended GDD. In our case the GVD-compensated chirped mirror pair from Layertec[37] will introduce ~ -40 ± 20 fs^2 per bounce.

Compared to prisms and grating pairs, the chirped mirror pair is a compact and user-friendly device, with lower losses, increased bandwidth, improved control of higher order dispersion and higher stability.[34]

2.4 Stretcher-compressor assembly

As we have seen in Chap. 1, in CPA the optical pulses are stretched and, after the amplification, the dispersion introduced by the stretcher must be compensated with a matched compressor. Mainly, this can be done in two different ways, one that is the most common approach where normal dispersion is introduced – also called up-chirping the pulse – and then it is removed by inserting a dispersion with the opposite sign, i.e. anomalous dispersion or down-chirping the pulse (Figure 2.8). The other approach consists in doing the reverse (Figure 2.8).

Also, optical components commonly used for stretching and compressing pulses were described in the previous sections – glass blocks, grating pairs, prism pairs and chirped mirrors. Their dispersion terms were mathematically defined and we can summarize in general that information into positive or negative contributions. This will allow us to estimate whether there is sum or cancelation of dispersion parameters, which is fundamental when making a first selection of which components to use as a stretcher or compressor device, as shown in Table 2.3.

In this work we chose to up-chirp the pulse first and then to down-chirp it in a configuration that we presently describe. The pulse is initially stretched by crossing a

thickness of transparent material (a block of SF11 glass), introducing a large amount of positive GDD and TOD. A grating pair is chosen to compress it as it is highly dispersive and can easily compensate the GDD. However, as we have discussed before, for a pulse with a final duration of a few tens of femtoseconds not only the GDD but also the TOD must be considered and as we can observe in Table 2.3 grating pairs will add TOD to the pulse instead of reducing it. Then, prism pairs can be used together with gratings to compensate all the TOD and part of the GDD – although they are less dispersive they will also introduce GDD dispersion with the same sign. The combination of prisms and gratings as GDD compensators has been successfully used[38] but requires special care when choosing the right parameters. Finally, at the end of the compressor line the remaining GDD can be finely compensated by using the chirped mirror pair.

To achieve the intended output pulse duration by using the setup described above, not only empirical characterization of all assembly must be done but also each of the optical components should be individually characterized. For the characterization we chose to measure the actual effect of each device on the duration of a short laser pulse passing through it, for different parameters. Since the pulse duration measurement relies on specific diagnostics, the next chapter will be dedicated to discussing them.

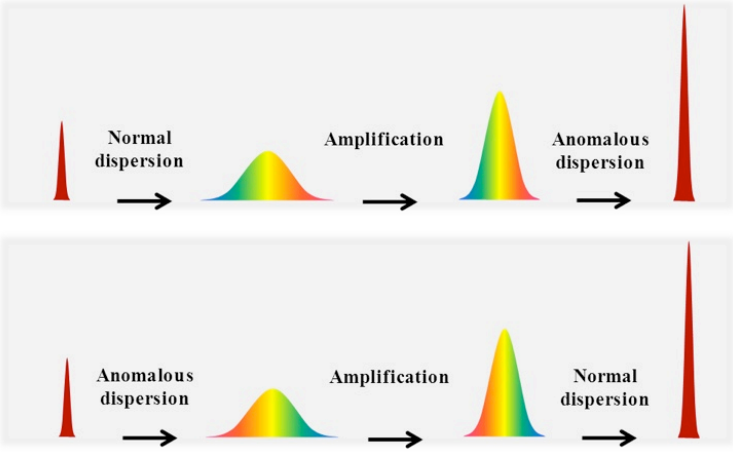

Figure 2.8: Schematic representation of the two principles of stretching and compressing the pulse. Upper box: insertion of positive GDD and down-chirp compensation (configuration used in this work); lower box: initial negative GDD is cancelled by an up-chirp compressor.

Table 2.3: Sign of dispersion contributions of the most common optical components of a stretcher-compressor assembly.

	GDD	TOD
Transparent material	+	+
Grating pair	-	+
Prism pair	-	-
Chirped mirrors	-	**0**

3

Ultrashort Pulse Characterization

The generation of ultrashort pulses and their increased utility in fundamental and applied sciences in the last decades led to the development of new measurement techniques,[23,24,39,40] since conventional diagnostic techniques were not suitable to measure these very short events. In fact, even today the fastest photodiodes and sampling oscilloscopes are limited to the several picosecond regime thus having temporal responses several orders of magnitude larger than the duration of ultrashort pulses. Indirect and nonlinear optical methods were proposed – such as the pulse autocorrelation – for time domain characterization, and spectrometers were used separately to measure the spectrum of optical pulses, operating in the frequency domain. However, the full characterization of the electric field of an ultrashort laser pulse was not possible through these techniques and it was only recently that the introduction of time-frequency methods allowed this characterization. Among these techniques, frequency-resolved optical gating (FROG) is the most studied and established ultrashort pulse measurement technique.[40]

3.1 Autocorrelation

Autocorrelation[41] is a time-domain characterization technique that has been widely used since its first demonstration in 1966.[42] A large number of experimental implementations and variations of autocorrelators have been developed[40] and we can divide them in two main types, the intensity autocorrelators[23] and the interferometric autocorrelators.[23] Both methods use the pulse itself as a gating event to obtain an indirect measurement of its duration, since there are no shorter events than the ultrashort pulses themselves.

The main principle of autocorrelation consists in in the following steps:

- generating a replica of the pulse to be measure, by splitting it e.g. in a Michelson interferometer or equivalent configuration using a 50%/50% beam-splitter;[22]
- sending the pulses through distinct paths such that the length of one of them is adjustable;

- creating and detecting a signal whose intensity is proportional to the product of the intensities of the pulse replicas (for instance by creating sum-frequency generation in a nonlinear medium) and measuring the variation of that signal with the relative pulse delay.

Given the interaction geometry, this nonlinear medium is typically a second-harmonic generation (SHG) crystal for the original pulse wavelength.[24] In the case of the SHG crystal, a light with twice the frequency of the input light will be produced.

Autocorrelators can be found either in a collinear or noncollinear geometry,[24] resulting in respectively interferometric autocorrelator and intensity autocorrelator (Figure 3.1). The former are not background free as, using a collinear configuration, both the upconvertion of the two replicas of the pulse and the SHG signal are recorded[23] and since the latter only records the SHG signal it has the advantage of detecting any small pedestals or wings of the pulse[22] (Figure 3.2).

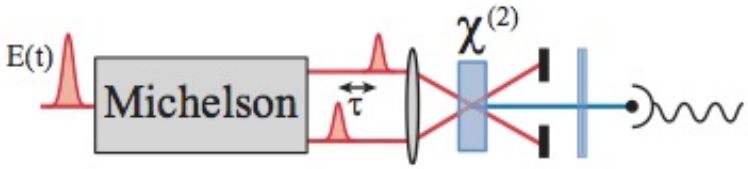

Figure 3.1: Schematic representation of an intensity second-harmonic autocorrelator using a Michelson interferometer and a SHG crystal. The pulse is split in two on a Michelson interferometer and is recombined in a second order nonlinear crystal generating a new signal.[23]

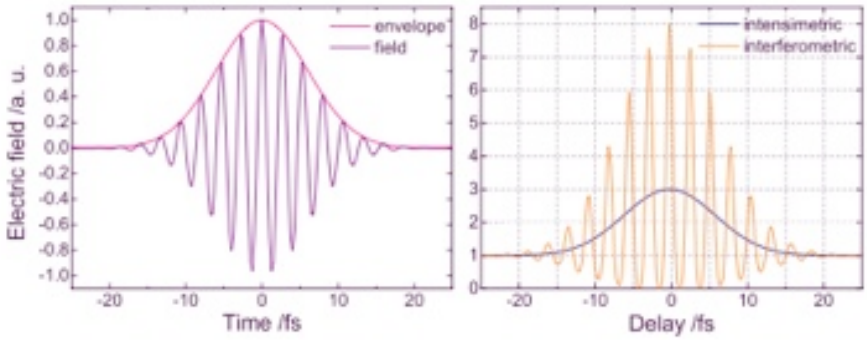

Figure 3.2: Examples of intensity and interferometric autocorrelations of a Gaussian pulse. Left box: graphic of a FTL Gaussian input pulse; right box: normalized fringe-resolved interferometric autocorrelation and intensity autocorrelation.[25]

To determine the pulse duration we must make an assumption about the shape of the input signal and use the known relation between the FWHM duration of the autocorrelation Δt_{AC} and the FWHM duration of the input pulse Δt corresponding to each shape. For instance, if a Gaussian shape is assumed we have:

$$\Delta t_{AC} / \Delta t = 1.414 \tag{3.2}$$

and for a hyperbolic secant squared the ratio is given by:

$$\Delta t_{AC} / \Delta t = 1.543 \tag{3.3}$$

We call these the deconvolution factors.[25]

Although we can easily and quickly estimate the pulse duration with autocorrelators they do not provide much more information than that. Even the fact that we must make an *a priori* assumption about their shape tells us that the data obtained is an approximation. In fact, only limited information on the pulse shape can be retrieved, since many symmetric and asymmetric pulse shape results in very similar symmetric autocorrelation traces[24] and even when the spectrum or another quantity, such as the interferometric autocorrelation, is measured the information is not sufficient to determine it.[40] These are called incomplete characterization methods, and to have further information methods with higher complexity and refinement must be used[23] as the one we will describe latter on this chapter.

3.1.1 Background-free intensity scanning autocorrelator

Intensity autocorrelators, as described previously, are background-free since the two time-delayed pulses are recombined noncollinearly, by focusing them at a mutual angle into the nonlinear crystal. Also, intensity autocorrelators work in a scanning mode as, by moving one interferometer arm, the autocorrelation intensity function will be reconstructed point by point. This was the type of autocorrelation chosen to estimate the duration of the chirped pulses in our work, given the simplicity of the setup described above (Figure 3.3).

The background-free intensity scanning autocorrelator (Figure 3.4) previously developed by our laser group consists in a beamsplitter that divides the input pulse in two. One pulse is back-reflected by a plane metallic mirror, and after being redirected by two additional mirrors, a concave metallic mirror sends it to the nonlinear crystal – a beta barium borate (BBO) crystal. The second pulse will be also sent to the same concave metallic mirror after being back-reflected by a corner-cube mirror, mounted on a controllable translation stage, and redirected by a metallic plane mirror. The translation stage allows varying its optical path length with respect to the other replica, and rather than doing this scanning manually with a micrometer head (also possible in our setup) we use a mechanical shaker driven by a trigger signal – a triangular wave derived from a waveform generator – that causes a periodic motion around the position where the two pulses overlap. After crossing the beams inside the crystal, sum frequency generation takes place and the signal is sent to a line mirror for the resulting green wavelength. After passing through a lens and another mirror the pulse reaches a photodiode tube and its output can be visualised in an oscilloscope (Figure 3.5). Before the photomultiplier, a plastic tube and an iris aperture blocks the room light and the remaining fundamental and frequency-doubled components.

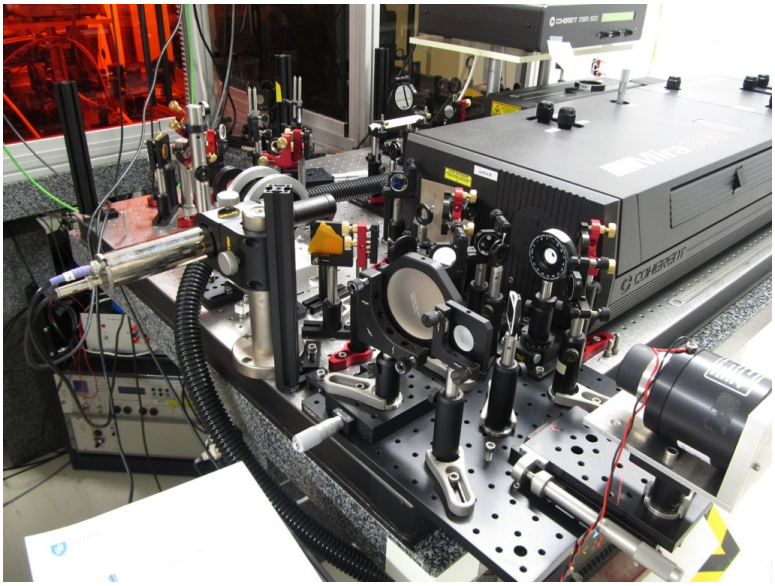

Figure 3.3: Experimental scanning intensity autocorrelator setup used to characterize the pulses from the oscillator. The input pulse is split in a Michelson interferometer, and thanks to a shaker the length of one arm is continuously changed. This allows the construction of the autocorrelation function after recombining the pulses in a second order nonlinear crystal.

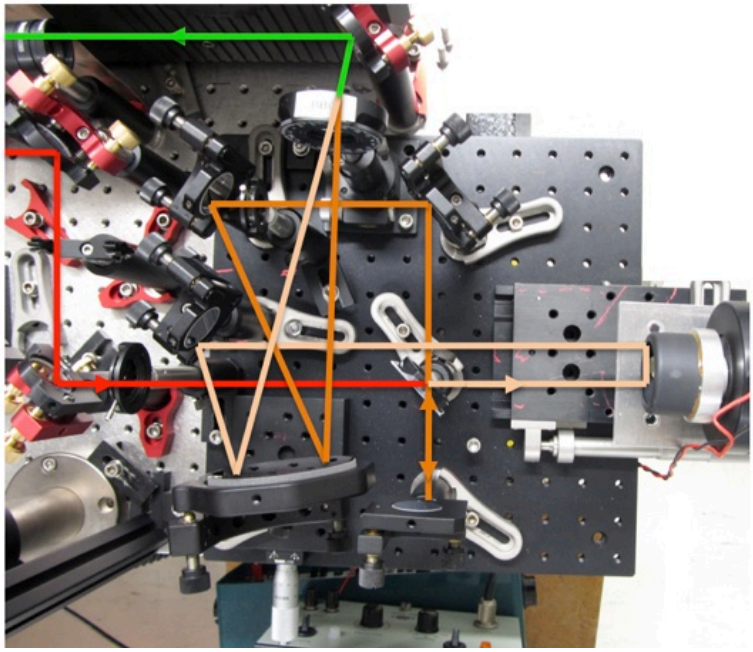

Figure 3.4: Schematic representation of the optical path of the pulses on the scanning intensity autocorrelator setup used to characterize the pulses from the oscillator. The input pulse (red) is split in two: one part goes through a fixed path length (orange) and the other suffers a periodically delay caused by a mechanical shaker (salmon); after crossing both parts inside a nonlinear crystal the SHG is generated (green) and is sent to the photomultiplier.

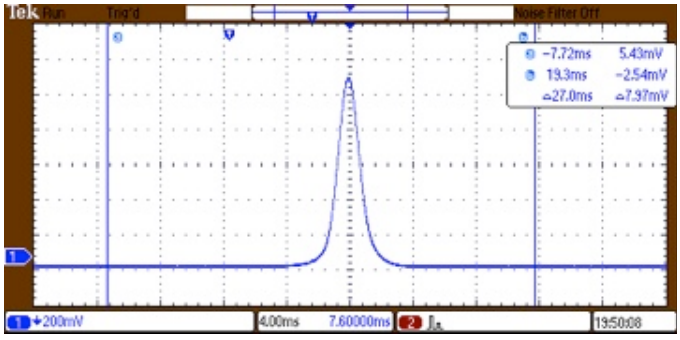

Figure 3.5: Example of a visualised autocorrelation on the oscilloscope display. The superposition of the two pulses in the nonlinear optical medium produce a slow (ms-scale) detection signal that corresponds to a coherent addition of both the electric fields.

3.2 Frequency-resolved optical gating

As we have stated in previous chapters, pulse stretching and compression are only possible by the introduction of dispersion. Also we have written that the dispersion of an ultrashort laser pulse may be described by its spectral phase, which is normally expressed as a Taylor series around the central frequency containing different order terms and that we should determine those terms, especially the GDD and TOD in our case, if we intend to compress the pulses to their Fourier-transform limit. While the above method can only give an estimate of the pulse duration or of the pulse intensity envelope, complete characterization techniques allow for the full reconstruction of the pulse electric field $E(t)$ once both the spectral amplitude $A(\omega)$ and the spectral phase $\phi(\omega)$ can be retrieved.

It was not until recently that several complete characterization techniques have emerged.[40] FROG is one of those new pulse measurement techniques that allows for both the measurement of the amplitude and the spectral phase of the pulses[5] and it has become the most popular time-frequency method since its invention in 1991.[43] In fact, with this technique we can easily measure different pulse lengths, even the shortest ones – pulses with less than 5 fs have been successfully measured with FROG[44] –, with the advantage that it can go through a wide range of wavelengths – from the mid-infrared to the extreme ultraviolet and much more recently in the x-ray regions of the spectrum[45] –, and it can measure even complex pulses. Moreover it is also a robust, accurate and rigorous method.[40]

Basically, this technique consists in generating as a spectrogram and is based on the following steps:

- temporally slicing the pulse we intend to measure with a gate pulse, which can be either a variable delayed replica of the test pulse or a different pulse;
- mixing the two pulses inside an instantaneous nonlinear optical medium;
- spectrally resolving the resulting frequency up-converted signal[24] (Figure 3.6), thus obtaining the *measured FROG trace*;

- applying a sophisticated iterative pulse-retrieval algorithm that will determine the input pulse spectral amplitude and phase by comparing it with a *retrieved FROG trace.*

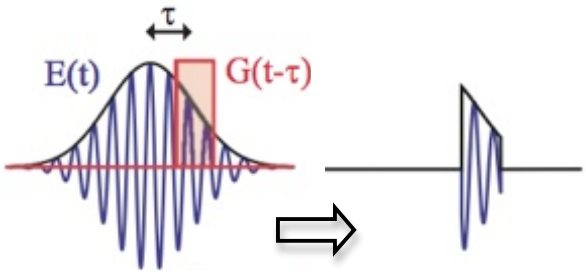

Figure 3.6: Schematic representation of the frequency-resolved optical gating main principle. The test pulse *E(t)* and the gate pulse *G(t-τ)* interact inside a nonlinear medium (left) slicing the test pulse (right).[23]

The FROG trace I_{FROG} is a 2D signal – a spectrum of the gated pulse as a function of the delay τ – and can be expressed by:

$$I_{FROG}(\omega,\tau) = \left| \int E(t)G(t-\tau)e^{-i\omega t}dt \right|^2 \tag{3.4}$$

3.2.1 Second-harmonic generation FROG

Different FROG geometries have been developed[40] being second-harmonic generation frequency-resolved optical gating (SHG-FROG) a widely employed method[24] and the one that we intend to use in our work. SHG-FROG, being based on a second-order nonlinearity, is a very sensitive technique compared to other FROG geometries, such as those based on much weaker third-order optical nonlinearities.[40] This results in a detection signal with higher energy in SHG-FROG than in other FROG geometries for the same amount of input pulse energy. It also uses a standard SHG-based noncollinear intensity autocorrelator, which instead of using a photodiode as a detector is spectrally resolved (Figure 3.7) and so we can easily adapt the chosen and available autocorrelator in our laboratory described in Sec. 3.1.1 to take the complete measurements of the chirped pulses.

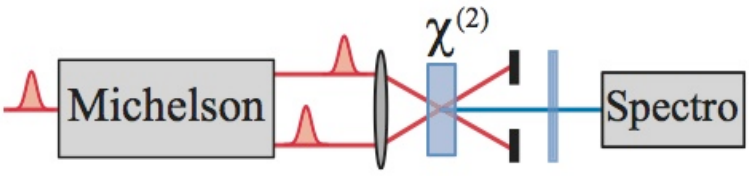

Figure 3.7: Schematic representation of a second-harmonic generation frequency-resolved optical gating using a Michelson interferometer and a SHG crystal. The SHG-FROG consists in a standard SHG-based noncollinear intensity autocorrelator with photodetector replaced by a spectrometer.[23]

The SHG-FROG trace $I_{SHG\text{-}FROG}$ results from a similar relation written in Eq. (3.4) where the gate pulse is the delayed pulse itself:

$$I_{SHG-FROG}(\omega,\tau) = \left| \int E(t)E(t-\tau)e^{-i\omega t}dt \right|^2 \tag{3.5}$$

Like before we have a 2D output signal allowing us to plot the spectral phase versus the delay (Figure 3.8) and to easily determine the contribution of the GDD and TOD on the chirped pulse. However, it has a significant disadvantage when compared to other FROG geometries: when using the pulse as its own test gate, the SHG-FROG traces always result symmetrical with respect to the imposed delay, thus resulting in direction of time ambiguity[24,40] (Figure 3.9). Nonetheless, this can be removed by simply placing a piece of glass before the beamsplitter that will introduce a positive chirp or create satellite pulses via surface reflections.[24]

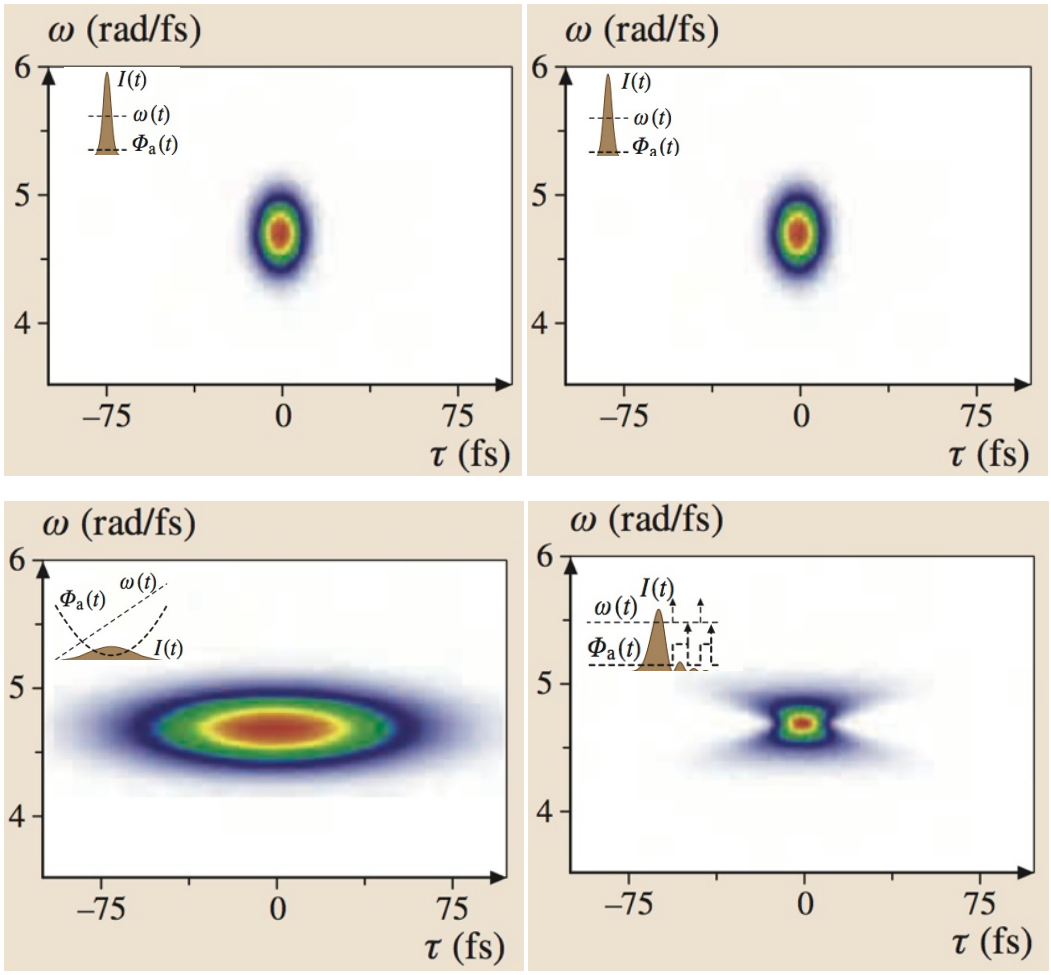

Figure 3.8: Examples of frequency-resolved optical gating trace for common ultrashort pulse distortions (shown on the top left of each box). Upper left box: FROG trace of a FTL 10 fs pulse; upper right box: FROG trace remains the same as only first order dispersion value was introduced; lower left box: second order dispersion term creates a FROG trace stretched in time (note that it is not possible to tell whether it is normal or anomalous dispersion); lower right box: FROG trace of a pulse with third order dispersion term gives us an unintuitive spectrogram since we have a symmetrical image.[24]

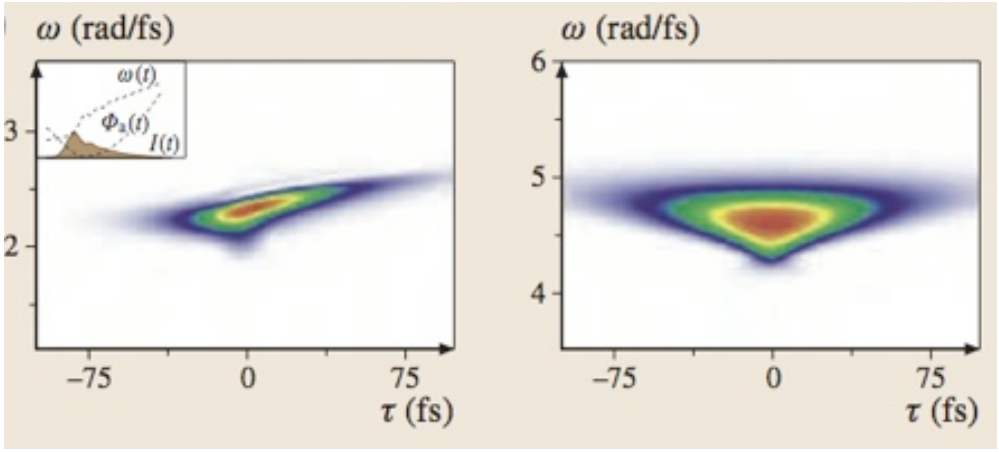

Figure 3.9: Examples of FROG traces of a pulse with GD, GDD and TOD using two different FROG techniques. Left box: FROG trace using polarization gate FROG; right box: using SHG FROG it is not possible to distinguish between positive or negative GDD nor between pre- or post-pulses. [24]

4

Stretching and compression devices

As was previously mentioned in Chap. 2, for this project a transmission grating pair with 300 groves/mm will be used to compensate the larger amount of dispersion introduced by the SF11 glass block, together with a SF11 prism pair to compensate a moderate amount of dispersion. Gratings and prisms pairs are classical examples for stretching and compression and the combination of the two has already been successfully used to perform spectral phase compensation up to the 3rd dispersion order.[46] However, this combination requires a careful choice of the parameters for which the devices can make the desired compensation, since we are dealing with very broadband spectra for which even a small amount of these dispersion orders will cause a highly relevant increase on the duration of the pulse (Figure 4.1). For this reason, a preliminary study – either through numerical simulations or experimental characterization – of the light dispersion caused by each optical component alone using well know pulses is essential. One possibility is to use the mode-locked pulses generated at the oscillator at the beginning of the laser chain, since these pulses have undergone less optical phenomena than those exiting ahead of the laser chain, and try to compress them to their FTL duration.

4.1 Numerical simulations

As was written before, in order to characterize the dispersion caused by the most relevant optical components that will be placed on the final setup we started by using the available pulses that come directly from the oscillator, which seeds the OPCPA system (a fuller characterization of the oscillator may be found later on this chapter and the description of the OPCPA setup is made in Chap. 5). Assuming that these pulses have a Gaussian profile with ~60 fs FWHM FTL duration, a central wavelength of 1030 nm and a repetition rate of 76 MHz, we performed several simulations using two dedicated software programs, Disperse-O-Matic (DOM)[47] and *femto*Pulse Master (FPM)[48].

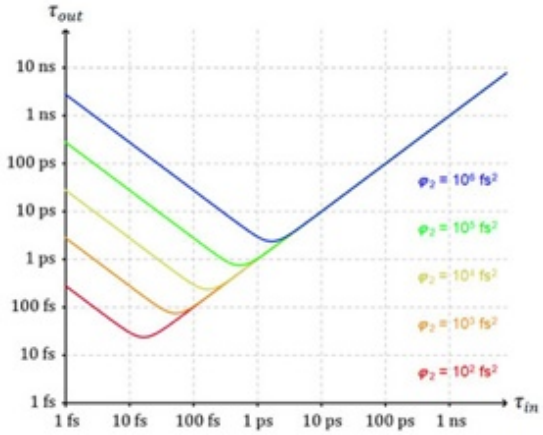

Figure 4.1: Output pulse duration versus initial pulse duration for different values of GDD. As the input pulse width becomes shorter, the effects of GDD become more pronounced, since the pulse broadening and chirping is stronger for pulses with broader bandwidths. (Note that the values in this graphic correspond to the FWHM pulse duration defined in our work as Δt).[49]

DOM is a free simulation software running inside a LabView code environment. It calculates both linear and angular dispersion caused by the most common optical devices, such as grating and prism pairs, and has a database of dispersion coefficients for a large range of optical media. It also allows combinations of these optical components thus simulating an all stretcher-compressor assembly, determining the overall dispersion and duration of the output pulse.

FPM is a commercial simulation software also running in a LabView environment, which simulates optical diagnostic techniques, for example autocorrelation and FROG, calculating in both the temporal and spectral domains. Thus, for a given input pulse we can easily obtain its temporal profile and final duration resulting from arbitrary amounts of introduced GDD and TOD.

In this section we will study the dispersion for each of the most relevant optical devices individually by using the above programs, considering mainly the order of magnitude of the dispersion resulting from single or multiple passes through the SF11 glass block.

4.1.1 SF11 glass block

The SF11 glass block (EKSMA Optics) that we will use to expand the pulses, already introduced on Chap. 2, is 12.5 cm long and it can be used in a single pass or multiple pass configuration according to the desired dispersion. For that reason it is useful recording the GDD and TOD introduced by this optical component, as shown in Table 4.1 (these values were determined directly from DOM software).

Also, as the oscillator is followed by an optical component, the Faraday isolator (FI, Leysop Ltd)[50] – consisting of two 1.2 cm thick Glan-Taylor calcite polarizers[51] (a total of

2.4 mm of calcite) and a 45° Faraday rotator made of 3.5 cm long terbium gallium garnet (TGG) crystal –, its material dispersion must be calculated and added to one generated by the SF11 rod (Table 4.1). This component is important and cannot be neglected as it is used to prevent backward pulses to go inside the cavity, avoiding instabilities and damage.

Thus, considering the values of the GDD introduced by the FI, by one to four passes in the SF11 rod and by both devices together we determined the output duration of the pulses also summarized in Table 4.1.

Table 4.1: Calculated dispersion coefficients and correspondent output pulse duration for an FWHM FTL = 60 fs introduced by the FI, by 1 to 4 passes through the 12.5 cm SF11 glass and by the FI together with the single and multiple pass through the SF11 glass block.

λ_0 1030 nm		ϕ_2 (fs^2)	ϕ_3 (fs^3)	τ (fs)
Oscillator		0	0	51
FI (2.4 cm of calcite + 3.5 cm of TGG)		5614.48	2734.42	226.2
SF11 glass block (12.5 cm)	1 ×	15715.96	14936.41	618.9
	2 ×	31431.92	29872.82	1234.7
	3 ×	47147.88	44809.22	1851.1
	4 ×	62863.83	59745.63	2467.7
FI + SF11 glass block	1 pass	21330.44	17670.83	838.7
	2 pass	37046.40	32607.24	1454.9
	3 pass	52762.36	47543.65	2071.4
	4 pass	68478.32	62480.06	2688.1

Next we studied the effect of these dispersion values on the pulse by using FPM. We started by determining the autocorrelation value of the input pulse with a zero phase, i.e. assuming the pulse as FTL. After this, since the majority of GDD values range from 10^4 to 10^5 fs^2 we simulated the autocorrelation for these two boundaries, and as expected we verified that this amounts of GDD will cause a relevant effect on the pulse that could be experimentally detected. We also determined what would be the minimum value of GDD for which we would start having measurable chirped pulses (i.e. the point where we could measure some significant difference between the autocorrelation of the input FTL and the output chirped pulse). We found that at a GDD of 10^3 fs^2 (i.e. already with the FI alone) we could measure a change in the pulse duration. These calculations

are summarized in Table 4.2 with the corresponding output duration determined using Eq. (3.2).

In what concerns the TOD, at 10^4 fs^3 we obtained almost the same autocorrelation value and at 10^5 fs^3 we verified that the pulse would be just a little longer than the input one (Table 4.2). Given these results we could conclude that using the pulses coming from the oscillator and working within the TOD values in Table 4.1 measurable effect to the pulse will be caused only by values closer to 10^5 fs^3, limiting the measurements to the introduced GDD.

Table 4.2: Calculated autocorrelation and output pulse duration (assuming a Gaussian profile) for the oscillator input pulses for different GDD and TOD values.

ϕ_2 (fs^2)	ϕ_3 (fs^3)	Δt_{AC} (fs)	τ (fs)
0	0	85.0	51.0
10^3	0	107.0	64.3
10^4	0	659.0	395.8
10^5	0	6535.6	3925.0
0	10^4	85.4	51.3
0	10^5	104.0	62.5

4.1.2 Transmission grating pair

The grating compressor works in a double pass configuration, as we have described previously on Sec. 2.3.2, and consists of two parallel, 25 mm × 25 mm near infrared transmission gratings (Thorlabs GmbH) with 300 grooves/mm and a blaze angle of 31.7°.[31] We have performed numerical simulations in DOM for this grating compressor with a fixed incident angle equal to the blaze angle at different distances between the gratings, Table 4.3 summarizes the most relevant results, which are those that corresponds to nearly opposite GDD values to those calculated in the previous section. Note that for a fixed angle the GDD or TOD change linearly with the grating separation, as shown in Figure 2.4.

Although gratings are very useful to compensate large amounts of GDD in a small distance, they have the inconvenient of adding TOD to the pulse that has been stretched by a transparent material, instead of cancelling it. As we can see the corresponding TOD is even higher than that introduced by 1 to 4 passes in the SF11 rod (Table 4.3) and thus at a certain point it can start to have an impact in the pulse requiring an extra compressor in order to cancel it. (Note that autocorrelations for the GDD values in Table 4.3 will be similar to the ones already determined in Tables 4.1).

Table 4.3: Calculated dispersion coefficients introduced by the grating pair compressor with an incident angle of 31.7° vs. perpendicular gratings separation L_g.

L_g (cm) ($\gamma = 31.7°$ at $\lambda_0 =$ 1030 nm)	ϕ_2 (fs^2)	ϕ_3 (fs^3)	(Compensates for:)
1.6	- 5988.911	9134.934	(FI)
4.2	-15720.89	23979.20	(12.5 cm)
5.8	-21709.80	33114.14	(FI + 12.5 cm SF11)
8.4	-31441.78	47958.40	(25 cm SF11)
10.0	-37430.69	57093.34	(FI + 25 cm SF11)
12.6	-47162.67	71937.61	(37.5 cm SF11)
14.2	-53151.58	81072.54	(FI + 37.5 cm SF11)
16.8	-62883.56	95916.81	(50 cm SF11)
18.4	-68872.47	105051.7	(FI + 50 cm SF11)

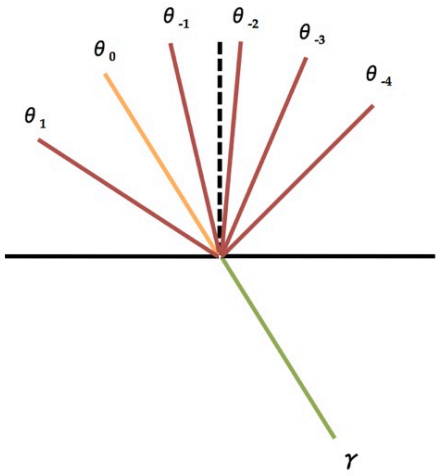

Figure 4.2: Schematic of the several orders of diffraction for a 300 g/mm transmission grating with an incident angle $\gamma = 32°$ at $\lambda = 1030$ nm. $\theta_1 = 57.03°$ $\theta_0 = 32°$ $\theta_{-1} = 12.76°$ $\theta_{-2} = -5.05°$ $\theta_{-3} = -23.4°$ $\theta_{-4} = -44.92°$; with θ_{-1} being the most efficient diffraction order.

Also we have determined the angles for the various orders of transmission θ_m of the 300 g/mm grating at 1030 nm with an incident angle γ equal to 32° [52] (we work with an approximation of the blaze angle of 31.7°) and we obtained the most efficient order at 12.76° (Figure 4.2), note that this is in accordance to Eq. (2.25). Figure 4.3 shows the layout of the grating compressor taking into account the angle of the most efficient order and the distance needed to compensate the GDD generated by the FI together with the

SF11 rod in a double pass. The first grating diffracts the incident beam in various orders however since the most efficient is at 12.7° the second grating is placed at that direction; the beam lives the second grating with the same angle as the incident angle γ and is sent backwards by a metallic mirror.

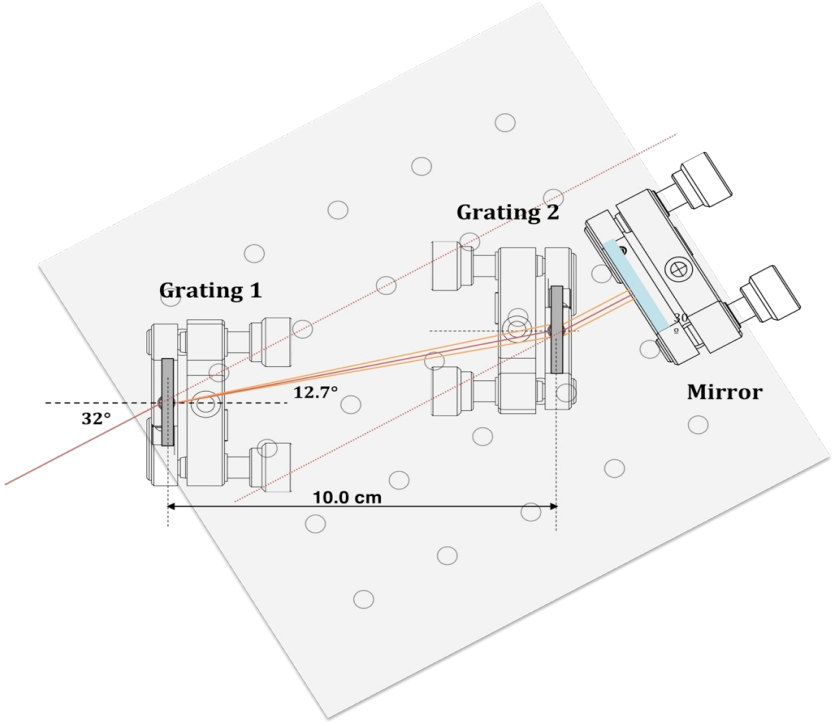

Figure 4.3: Layout of the 300 g/mm grating pair compressor with $\gamma = 32^{o}$ at $\lambda = 1030$ nm.

4.1.3 SF11 Brewster prism pair

The prism compressor also works in a double pass configuration (cf. Sec. 2.3.3), and consists of two SF11 prisms with an apex angle of 59° (EKSMA Optics).[53] The first prism has a 25 mm side length prism and a thickness of 18 mm, with a beam aperture of 12.0 mm; the second has a 50 mm side length and a thickness of 25 mm, with a beam aperture of up to 22.0 mm. We have used DOM to performed numerical simulations for different apex-to-apex distances between SF11 prisms with 59° apex angle, considering that the wavelength that crosses the apex of the second prism is of 1000 nm. This is approximately the shortest wavelength for the considered bandwidth of our beam, meaning that all the beam is passing through the prism aperture, while simultaneously having a minimum optical path inside the second prism (see Table 4.4).

Prisms are mainly useful for compensating higher orders of dispersion such as the TOD, and they have the main disadvantage of requiring very large distances to compensate large amounts of GDD, as is the case. From Table 4.4 we can see that instead of the 1.6 cm distance determined before for a grating compressor to compensate the GDD generated by the FI we have now a 48.6 cm apex-to-apex distance. To compensate both the FI and one pass of SF11 rod, almost 2 m of apex-to-apex distance is needed, meaning

that for larger GDD amounts such as those introduced by more passes through the SF11 rod the setup will be far from compact. Note that these values were determined considering a minimum prism thickness: if we add extra material dispersion caused by the SF11 glass crossed by the beams inside the prisms the required distance will be longer (see Table 4.5). Thus, considering that the main goal on using the prisms is to compensate partially the GDD and not all of it, and that very large distances between prisms will not only require more space but also higher collimation and stability of the beam (or even a larger second prism), we will characterize it under apex-to-apex distances of 2 m. However even this distance requires a large setup and so, a compact prism pair geometry was implemented such that a significant part of the required apex-to-apex distance is achieved through multiple reflections between two parallel large mirrors (Figure 4.4).

Table 4.4: Calculated dispersion coefficients introduced by the SF11 prism pair compressor with an apex angle of 59°, 1000 nm wavelength at apex vs. apex-to-apex distance L_p.

L_p (cm) (λ_0 = 1030 nm)	ϕ_2 (fs^2)	ϕ_3 (fs^3)	(Compensates for:)
48.6	-6004.174	-13708.12	(FI)
127.5	-15719.35	-35888.81	(12.5 cm)
176.8	-21797.49	-49765.82	(FI + 12.5 cm SF11)

Table 4.5: Calculated dispersion coefficients introduced by the SF11 prism pair compressor with an apex angle of 59° vs. apex-to-apex distance L_p and SF11 crossed length l_m.

L_p (cm) (λ_0 = 1030 nm)	l_m (cm)	ϕ_{2a} (fs^2)	ϕ_{2m} (fs^2)	ϕ_2 (fs^2)	(Compensates for:)
54.4	0.5	-6706.921	628.6383	-6078.283	(FI)
59.5	1.0	-7335.695	12572.77	-6078.418	
79.9	3.0	-9850.791	37718.30	-6078.960	
132.60	0.5	-16348.12	628.6383	-15719.48	(12.5 cm)
137.7	1.0	-16976.89	12572.77	-15719.62	
158.1	3.0	-19491.99	37718.30	-15720.16	
181.9	0.5	-22426.27	628.6383	-21797.63	(FI + 12.5 cm SF11)
187.0	1.0	-23055.04	12572.77	-21797.76	
207.4	3.0	-25570.14	37718.30	-21798.31	

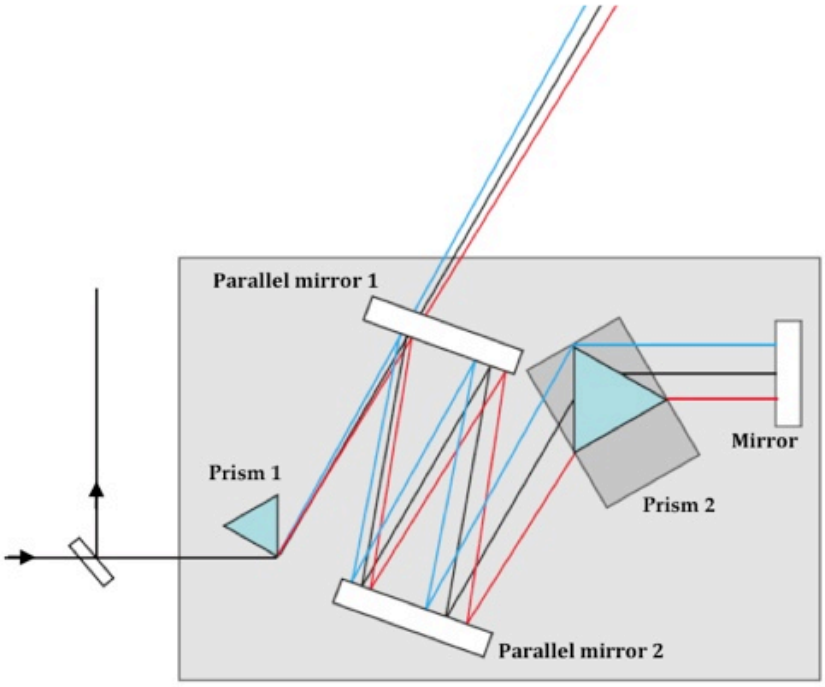

Figure 4.4: Prism compressor compact geometry.

4.2 Experimental characterization

For the experimental measurements we aligned the background-free intensity scanning autocorrelator available at L2I, already described in Sec. 3.1.1, near the oscillator output, we choose the most appropriate detector – a photomultiplier (QL30F, Thorn EMI Electron Tube) – and connected it to a digital oscilloscope (Tektronix DPO2014).[54] We proceeded to set up different configurations in order to characterize the stretching and compressing components individually and to perform some improvements while dealing with experimental problems. Output spectra of these setups were also measured with a USB spectrometer (USB 2000+ Ocean Optics).[55]

Previous measurements performed for the study of one, two and four passes through the SF11 rod led us to two important considerations that was taken in account in the experimental approaches described in this section:

- one was that to large values of autocorrelation could be associated a larger error (the empirical error for autocorrelation measurements is ~5-10%) which made us change the experimental approach of characterizing individually each optical component for a stretcher-compressor assembly with a minimum number of optical devices towards a more integrated approach where the resulting autocorrelations would be closer to the pulse FTL durations;
- the other was that oscillator could be delivering chirped (either be normal or anomalous) pulses leading to a different output duration of these

stretcher-compressor assembly. The importance of determining the absolute value and signal of the GDD delivered by the oscillator motivated its full characterization.

4.2.1 Oscillator

The oscillator used to seed the laser chain is a commercial Ti:sapphire Kerr-lens mode-locked oscillator (Coherent Mira 900 F)[56] and is composed by three main parts (Figure 4.5): the amplification medium – a Ti:sapphire rod; the mode-lock starting mechanism made of fused silica; and the prism compressor. And although the first two components are fixed, we can vary the prism compressor (specifically we can vary the insertion of the prisms) resulting in different GDD and TOD values.

Thus, in order to characterize the pulse we measured not only its output duration through the autocorrelation but also related it with the prism compressor (note that the FI was not included). For this purpose we had translated only the second prism (Figure 4.6) by rotating its translation stage mechanism in order to change the material insertion in the intra-cavity prism compressor. For each complete rotation of this mechanism we measured the corresponding autocorrelation value and spectrum, starting from the initial position.

Since for the different autocorrelation values the only parameter that is changing is the insertion of material we can write the total GDD ϕ_{2osc} as:

$$\phi_{2osc} = \phi_{2c} + 2\phi_{2m}\Delta x \tag{4.1}$$

where ϕ_{2m} is the dispersion caused by the insertion of 1 mm of prism material that when multiplied by the total thickness crossed by the beam inside the prism in a double configuration ($2\Delta x$) will give the material dispersion caused by the prism insertion and ϕ_{2c} is the sum of the constant GDD introduced by the fixed optical components. Note that the dispersion caused by the first prism material is included in this last constant. Also we have considered the angular dispersion caused by the prisms compressor to be constant, since a very small change is done in the apex-to-apex distance between prisms and that the angular dispersion for an increase of 1 mm is negligible when compared to material dispersion.

Thus, replacing Eq. (4.1) in Eq (2.11) we obtained the following:

$$\tau_{out} = \tau_{in}\sqrt{1+\left(2\frac{\phi_{2c}+2\phi_{2m}\Delta x}{\tau_{in}^2}\right)^2} \tag{4.2}$$

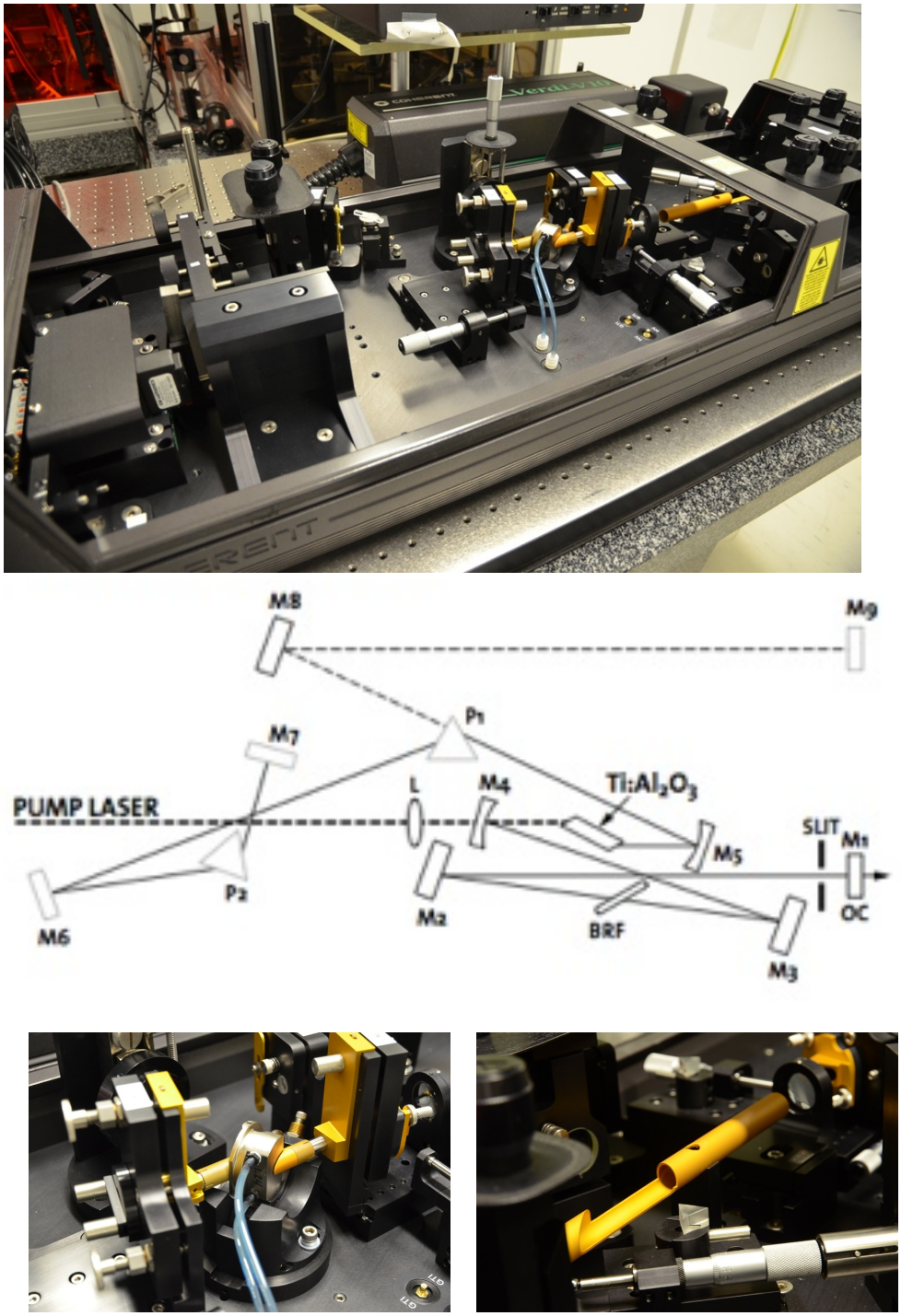

Figure 4.5: Oscillator Coherent Mira 900 F. Top box: Ti:sapphire laser cavity pumped by a Verdi-V 10; middle box: schematic representation of the oscillator cavity (M – mirror; P – prism; L – lens; BRF – birefringent filter; OC – output coupler);[56] left bottom box: Ti:sapphire crystal mount; left bottom box: prism compressor.

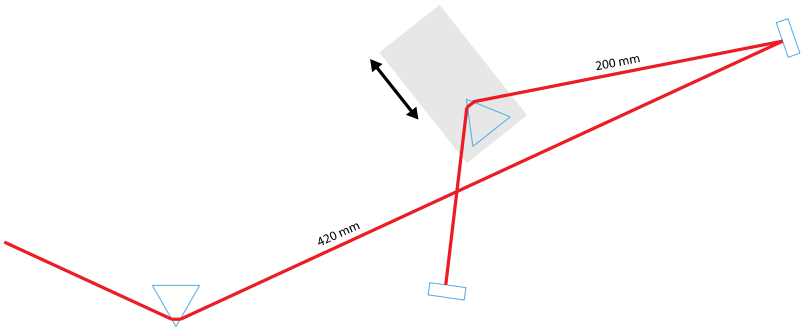

Figure 4.6: Optical path in the prism compressor inside the oscillator. Translating the second prism in the same direction of its main axis will insert or remove material dispersion that can change the output of the prism compressor.

However, fitting the data using Eq (4.2) we obtained parameters with large uncertainty associated and once our main goal was not to characterize the oscillator but having an order of magnitude of the GDD it was generating, we worked with a linear approximation. In fact, for $\phi_2/\tau_{in}^2 >> 1$ we obtain:

$$\tau_{out} = 2\frac{\phi_{2c}}{\tau_{in}} + 4\frac{\phi_{2m}}{\tau_{in}}\Delta x \tag{4.3}$$

For this purpose we calculated the theoretical values considering that the prisms were made of SF10 since scientific papers refer the prism material inside a Coherent Mira 900 as SF10 glass[35,57] what corresponds to a ϕ_{2m} = 105.9 fs^2/mm at a central wavelength of 1030 nm. Thus, for the constant dispersion inside the cavity caused by the sum of the various optical elements we obtained ϕ_{2c} = -2982.3 fs^2 (see Table 4.6). Finally, through the measured spectrum with a bandwidth of 24.3 nm we obtained an FTL duration of τ_{in} = 54.5 fs. Using Eq. (4.2) we determined the theoretical points for the same measured Δx and fitted it with the linear approximation of Eq. (4.3). Then, we adjusted the parameters of the experimental linear equation to the theoretical points minimizing the error between them (Figure 4.7). The obtained parameters were: ϕ_{2m} = ~97.9 fs^2/mm which matches with several well known optical media as for example SF1 (101.72 fs^2/mm), SF8 (110.78 fs^2/mm), SF10 (105.91 fs^2/mm), SF15 (95.49 fs^2/mm), SF52 (92.1 fs^2/mm); ϕ_{2c} = ~-3099 fs^2 that matches with the calculated GDD; and τ_{in} = ~51.85 fs that corresponds to a theoretical spectrum with a bandwidth of 25.8 nm, which is close to determined bandwidth of 24.3 nm. The measured region of the data, the experimental linear fit and the experimental curve can be found in Figure 4.8 (and also the experimental GDD) justifying the performed linear approximation with an inherent error.

The two parameters ϕ_{2m} and ϕ_{2c} give us for the first measured position (Δx = 6.19 mm) a ~-1888 fs^2 residual GDD, i.e. the value of GDD that is not compensated inside the cavity ϕ_{2osc}, through Eq. (4.1). This confirms that the pulse is leaving with a significant chirp and that this is also an anomalous one.

Table 4.6: Theoretical values for different optical elements in order to determine the total constant value of GDD inside the oscillator.

Element	ϕ_2 (fs^2/mm)	l (mm)	ϕ_2 (fs^2)
SF10 prism pair (angular GDD)	-8.947	620	-5547.1
SF10 first prism (material GDD)	105.91	5.40	571.9
Sapphire rod	32.19	2×23.0	1480.7
FS starting mechanism	18.97	27.0	512.2
Positive total	–	–	2564.8
Net TOTAL	–	–	-2982.3

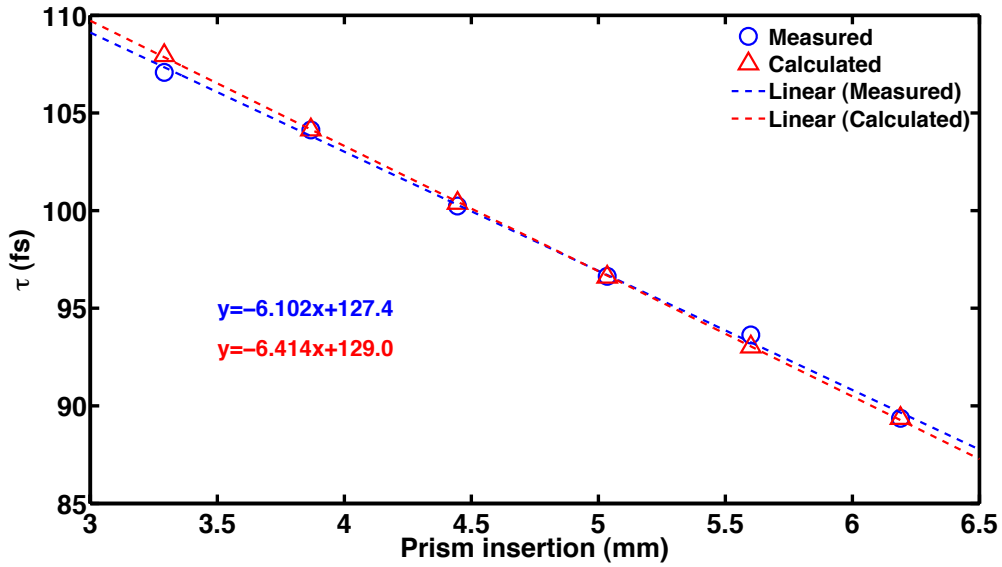

Figure 4.7: Calculated (red) and measured (blue) values of the output pulsewidth for the different measured prism insertion quantities. Linear fit of the calculated (dashed red line) and measured (dashed red blue) is also shown.

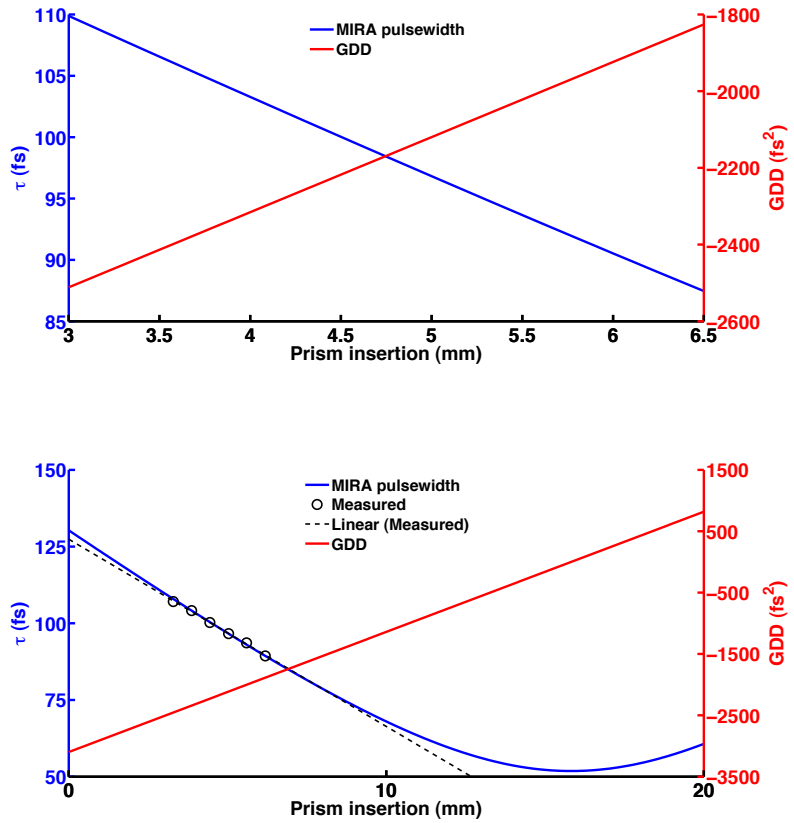

Figure 4.8: Variation of the GDD (red) and output durations (blue) with prism insertion. Top box: Variation of the GDD and output durations with prism insertion in the region of the experimental data; bottom box: variation of the GDD and output durations with prism insertion in large range. The measured points (black circles) and the experimental linear fit (dashed black line) can be compared with the experimental output duration vs. prism insertion curve.

4.2.2 Oscillator and FI

After the characterization of the oscillator we inserted the FI in the setup in order to characterize it. The FI will generate a positive GDD since it will cause only material dispersion, which we have already calculated in Sec. 4.1.1 (see Table 4.1) to be 5614.5 fs^2. Thus, if the pulses coming from the oscillator have a negative residual GDD (-1888 fs^2) after passing through the FI it will result in the cancelation of this negative GDD and an add of positive dispersion leading to a pulse normally dispersed of 4198 fs^2.

Analysing the measured autocorrelation for this setup, that was of ~344.2 fs we obtained a τ = ~206.7 fs output pulse duration. Considering the FTL pulse determined before (τ_{in} = 51.85 fs) we calculated through Eq. (2.11) that the measured output duration will correspond to a final GDD of ~5190 fs^2 – this means an experimental GDD for the FI of ~7078 fs^2. Thus, comparing the experimental GDD of the pulse after leaving the FI value with the theoretical one we have a difference of 992 fs^2 which could mean that the FI could be in fact generating more GDD than theoretically determined. In order to

understand this difference we searched in the literature about the TGG and we found only two references, one that gives us a value lower than the calculated through DOM however it considers only one axis[58] and a second that has very different values from the ones in the article.[59] Since the pulse is rotating 45º inside a magnetic field and different axis of the material generate different dispersion values we have no way to determine its precise value. However, once again it was not a main goal to characterize the FI but to have an order of magnitude of GDD of the pulse that leaves this component and also to have a measurement in accordance with the conclusion achieved previously about the residual negative chirp of the pulses coming from the oscillator.

4.2.3 Oscillator, FI, double pass in SF11 rod and transmission gratings

Having determined the GDD generated by the oscillator and the output of the oscillator together with the FI we moved for the characterization of the transmission gratings. The approach to studying the grating compressor consisted in stretching the pulse with the grating pair and compressing it with a double pass in the SF11 rod (Figure 4.9). Note that we were now using a configuration of up-chirping and down-chirping the pulse but in terms of measuring the residual GDD there is no difference. Also note that one pass on the rod will require a compressor with a very small distance, which could bring some difficult in manipulating the compressor and since to compensate the GDD generated by 25 cm of SF11 together with the FI we need ~10 cm perpendicular distance between gratings (see Table 4.3), what is already a comfortable distance, we choose to work with a double pass configuration.

In order to measure the autocorrelations of the output pulses after implementing all the setup and ensuring that we were having Gaussian autocorrelations, we proceed to a fine adjustment of the position of the second grating fixed in a translation stage finding the precise distance at which the autocorrelation was at a minimum. We then chose a distance range with the one corresponding to the minimum in the middle and recorded the autocorrelations values versus the position. Previous measurements to the ones described in this section showed several unexpected relative minimum and maximum values for the measured output duration vs. distance between gratings and this was only corrected once we have changed the direction of the translation stage. Before, the second grating was moving parallel to the incident direction and now the translation stage was fixed more a less with the same direction of the beam path performed between gratings (this is with 12.7° from the incident direction) (Figure 4.9).

Similarly to Eq (4.1) we can write the total GDD ϕ_{2total} as:

$$\phi_{2total} = \phi_{2c} + \phi_{2g}\Delta x \tag{4.3}$$

where ϕ_{2g} is the dispersion caused by the optical path between gratings increasing in 1 mm that multiplied by the total optical length between gratings (Δx) will give us the total angular dispersion and ϕ_{2c} is the sum of the GDD values introduced by the fixed optical

components that remains always constant. Note that now this include the residual GDD of the oscillator, the GDD introduced by the FI and also by the two passes in the SF11 rod. Thus, we have:

$$\tau_{out} = \tau_{in}\sqrt{1+\left(2\frac{\phi_{2c}+\phi_{2g}\Delta x}{\tau_{in}^2}\right)^2} \tag{4.4}$$

Through Eq. (4.4) we fitted the experimental data (Figure 4.10) (we chose to perform this fit only to the central measured values once the other ones correspond to higher autocorrelations values and thus to higher uncertainty). The obtained parameters were: ϕ_{2g} = ~-379.0 fs^2/mm which matches with theoretical value calculated through DOM (-375.5 fs^2/mm); ϕ_{2c} = ~-36360 fs^2 that matches with the overall GDD after the FI determined in the previous section (5190 fs^2) together with the GDD generated by 2 passes in the SF11 rod (31432 fs^2, listed in Table 4.1) which results in 36622 fs^2; and τ_{in} = ~70.07 fs was higher than the determined in Sec. 4.2.1 (51.85 fs).

In order to understand the difference in the FTL duration we studied the effect of the theoretical TOD since now we were having two high dispersion devices together introducing positive TOD, the grating and the rod. Thus, we started by calculating how much TOD the oscillator could be delivering performing the sum of the TOD generated by the various optical elements inside the cavity (see Table 4.7) and we obtained ϕ_3 = -6030.0 fs^3. Also from Tables 4.1 and 4.3 we have the TOD introduced by the FI (2734.4 fs^3), the 2 passes in the SF11 rod (29872.8 fs^3) and the grating pair with a perpendicular distance of 10 cm (57093.3 fs^3). Computing all these values we obtained a total of 95730.5 fs^3, which is of the order of magnitude that we already have shown to be significant in the pulse duration (see Sec. 4.1.1).

Thus, considering now from Eqs. (2.15) and (4.3) that we have:

$$\tau_{out} = \tau_{in}\sqrt{1+\left(2\frac{\phi_{2c}+\phi_{2g}\Delta x}{\tau_{in}^2}\right)^2+\frac{1}{2}\left(2\frac{\phi_{3c}+\phi_{3g}\Delta x}{\tau_{in}^3}\right)^2} \tag{4.5}$$

where ϕ_{3g} is the TOD per mm caused by the grating separation Δx and ϕ_{3c} is the sum of the TOD values introduced by the fixed optical components, that remains constant. We performed a new fit using Eq. (4.5), however this time we have considered all the measured points (Figure 4.11) once the approximation was better than considering only the central points. We obtained for the GDD that: ϕ_{2g} = ~-374.6 fs^2/mm which matches well with the theoretical one (-375.5 fs^2/mm); and ϕ_{2c} = ~36140 fs^2 which matches with its corresponding theoretical value (36622 fs^2). For the TOD the obtained parameters were: ϕ_{3g} = ~538.5 fs^3/mm which is within the error when compared with the theoretical value (571.7 fs^3/mm); and ϕ_{3c} = ~25440 fs^3 that corresponds to the TOD inserted by the FI and 25 cm of SF11 rod which is also within the error when compared to the theoretical fixed TOD value (26577 fs^3). However the determined input pulse duration τ_{in} = 61.98 fs was now closer to the previous measurements (51.85 fs).

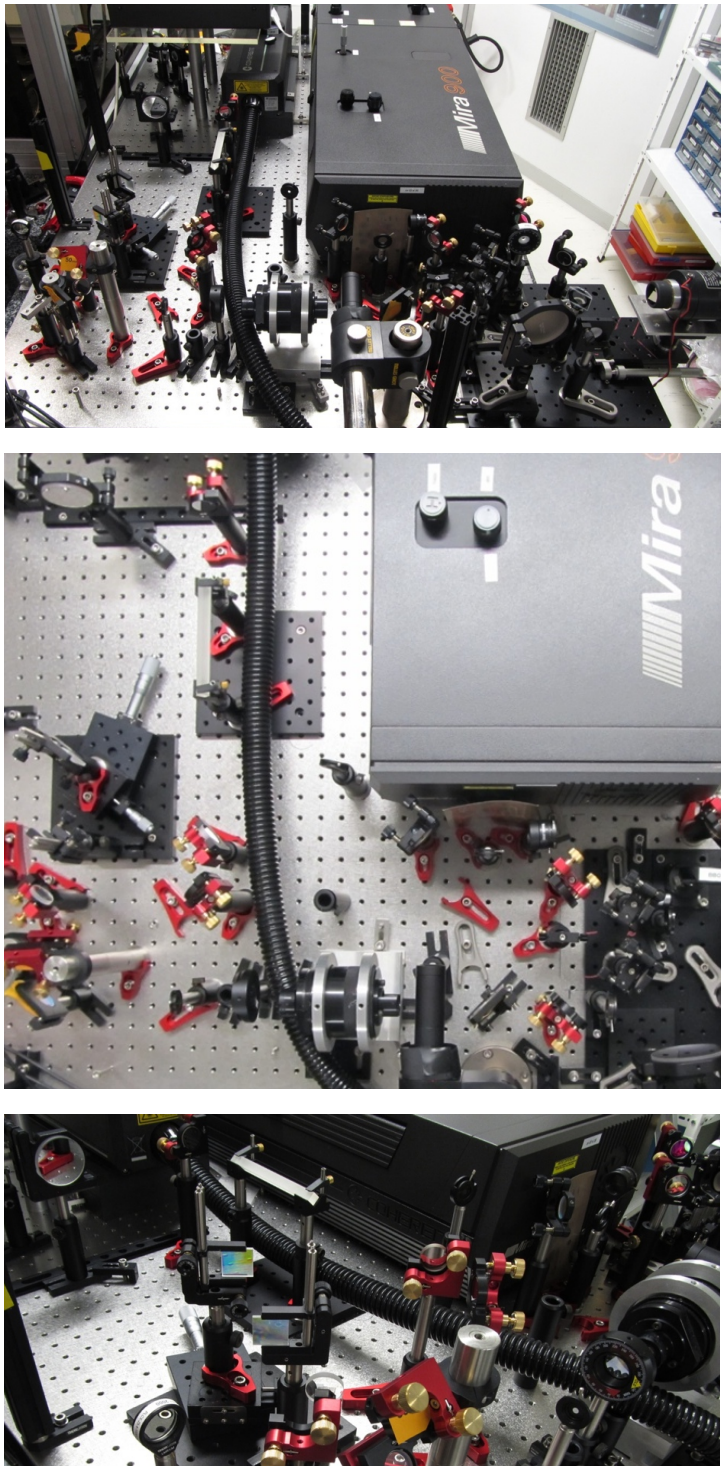

Figure 4.9: Experimental setup of the stretcher-compressor assembly to study grating pair. The pulse that leaves the oscillator pass trough FI, after in the grating compressor, then twice in the SF11 rod and finally they will be sent to the autocorrelator. The same setup is shown in different positions.

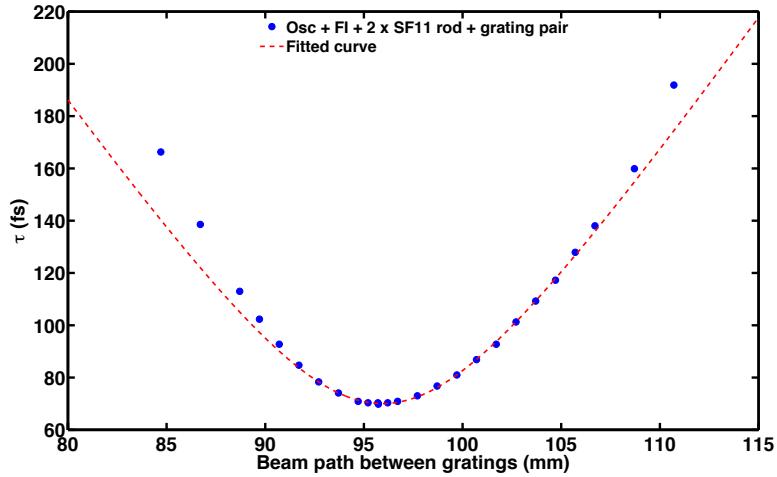

Figure 4.10: Experimental output pulse durations for different distances between gratings (blue points) and the corresponding fit (red line). This mathematical fit using Eq. 4.4 was done only for the central values once higher autocorrelations measurements have a large error associated.

The two parameters ϕ_{2g} and ϕ_{2c} give us for the position correspondent to the absolute minimum (Δx = 95.7 mm) a ~291 fs^2 residual GDD which is almost insignificant and thus we can consider that the value of GDD was compensated using the grating compressor. Also from ϕ_{3g} and ϕ_{3c} at the same position we have ~76974 fs^3.

Table 4.7: Theoretical values for different optical elements in order to determine the total constant value of TOD inside the oscillator.

Element	ϕ_3 (fs^3/mm)	l (mm)	ϕ_3 (fs^3)
SF10 prism pair (angular TOD)	-17.9	620	-11098.0
SF10 first prism (material TOD)	101.4	5.40	547.6
SF10 second prism (material TOD)	101.4	6.19	627.7
Sapphire rod	60.5	2×23.0	2783.0
FS starting mechanism	41.1	27.0	1109.7
Positive total	–	–	5068
Net TOTAL	–	–	-6030.0

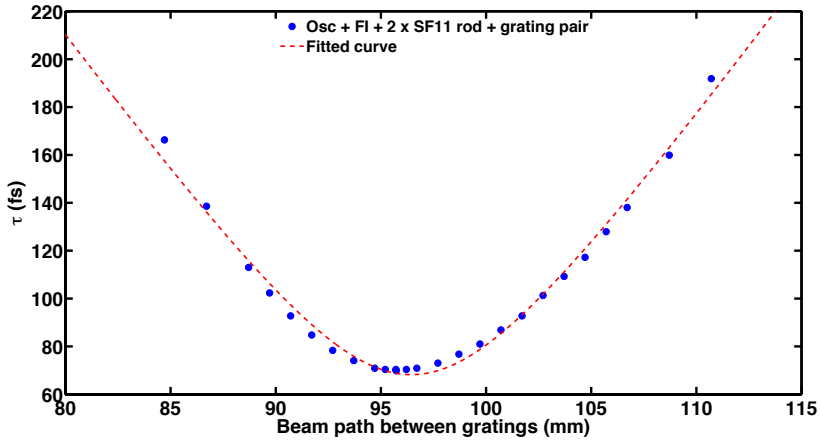

Figure 4.11: Experimental output pulse durations vs. distances between gratings (blue points) and the corresponding fit (red line). This mathematical fit considers also the TOD since the input pulse is only a few tenths of fs long and has a large TOD value.

4.2.3 Oscillator and prisms

In order to characterize the prism compressor we used a stretching-compressor assembly approach and since previous measurements using large distances between prisms to compensate the FI together with one pass in the SF11 rod led to several problems we chose to work with a simpler configuration with only the oscillator and the prisms, once with the material insertion of the second prism we could compensate the negative dispersion from the oscillator and from the angular dispersion of the prism pair (Figure 4.12).

After implementing the setup the procedure to acquire the autocorrelation values were similar to the one used for the gratings: we searched for the minimum autocorrelation, we chose a distance range such that the prism insertion corresponding to the minimum was in the central position, and we recorded the autocorrelation vs. the position of the second prism.

To determine the parameters we used Eq. 4.2 to fit the data where ϕ_{2m} is now the GDD per mm of SF11, which when multiplied by the total length crossed by the beam inside the prism in a double configuration ($2\Delta x$) will give us the prism material dispersion, caused by the insertion of this prism and ϕ_{2c} is the sum of the GDD values introduced by the oscillator and the angular dispersion of the prism compressor (Figure 4.13). The determined parameters were ϕ_{2m} = ~154.8 fs^2/mm which differs from the theoretical value (125.6 fs^2/mm); ϕ_{2c} = ~-4334 fs^2 which shows a difference from the correspondent theoretical value that results from the sum of the dispersion leaving the oscillator (-1888 fs^2) with the angular dispersion caused by a prism compressor with ~37 cm apex-to-apex distance (-4908 fs^2), i.e. -6792 fs^2 – this corresponds to an angular dispersion of ~-2446 fs^2 which for 37 cm will lead to an angular dispersion of ϕ_{2a} = ~-6.6 fs^2/mm (which is far

from the theoretical ϕ_{2a} = -13.3 fs^2/mm); and τ_{in} = ~60.05 fs which is in agreement with the FTL duration determined before.

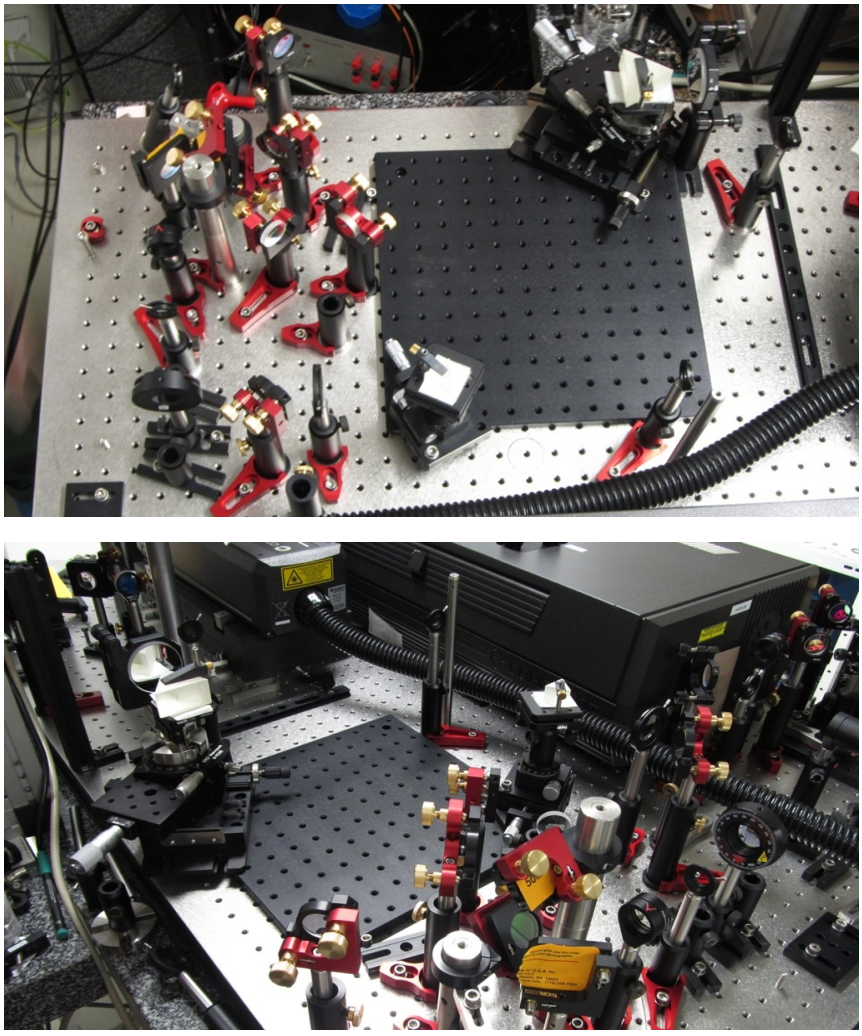

Figure 4.12: Experimental setup of the stretcher-compressor assembly to study prism pair. In order to understand the problems in the compression of the pulses using prism pair we chose to verify its capability in compressing a small value of positive dispersion introduced by the insertion of its own material thus the pulse that leaves the oscillator directly goes to prism compressor and then to the autocorrelator. The same setup is shown in different positions.

The difference in the GDD values ϕ_{2m} and ϕ_{2c} can be associated to the measurement of the prism insertion once its determination is not trivial and involves different parameters with associated errors. One is the direction of the translation stage of the prism which is approximately parallel to the prism main axis and thus a slightly difference between the two directions could be causing a variation in the calculus of the prism insertion quantities. Other is that the position reference correspondent to the point where the beam starts entering the prism lacks of precision since the beam has a significant diameter. And, finally, once the beam finds the prism with an incident angle not perpendicu-

lar to its main axis, extra geometrical considerations had to be done requiring the determination of the value of the incident angle which is experimentally difficult to measure and thus theoretical value need to be assumed considering the minimum deviation angle for the SF11 at 1030 nm.

The two parameters ϕ_{2m} and ϕ_{2c} give us for the prism insertion value correspondent to the minimum pulse duration (Δx = 14.2 mm) a ~-62 fs^2 residual GDD which is almost insignificant and thus, once again, we can consider that the value of GDD was compensated using the prism compressor.

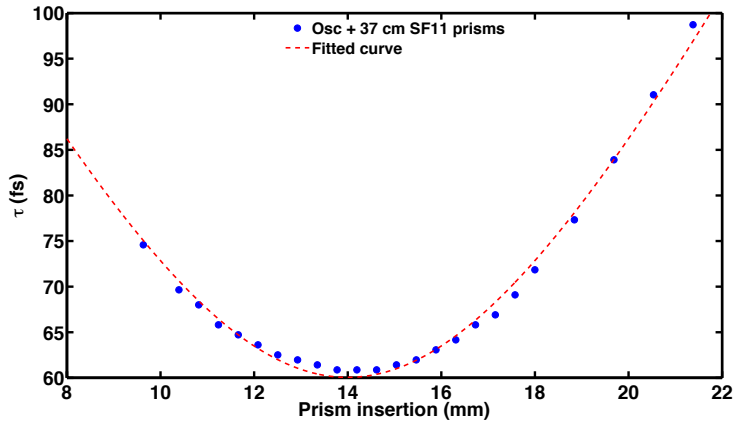

Figure 4.13: Experimental output pulse durations for different values of prism insertion (blue points) and the corresponding fit (red line).

4.2.4 Oscillator, FI and prisms

After a first characterization of the SF11 prism pair we inserted the FI in the experimental setup in order to find the origin of the problems detected while using large distances between prisms. In fact here the approach was the same as before however since more material dispersion was inserted by the FI a compressor with larger distance between prisms was required leading to a configuration with passes between prisms (a simpler version of the configuration already exemplified in Figure 4.4). And was just when we replace the two dielectric broadband mirrors used to perform the passes until now by two simple metallic mirrors that we finally obtained acceptable autocorrelations. Thus, the results shown in this section were already with this in consideration.

To determine the parameters we used once again Eq. 4.2 to fit the data (Figure 4.14) where the determined parameters were ϕ_{2m} = ~142.7 fs^2/mm which still differs, although closer than before, from the theoretical value (125.6 fs^2/mm); ϕ_{2c} = ~-4322 fs^2 which once again shows a difference, although closer than before, from the correspondent theoretical value that results from the sum of the dispersion leaving the FI (5190 fs^2) with the angular dispersion caused by a prism compressor with ~80 cm apex-to-apex distance (-10611 fs^2), i.e. -5421 fs^2 – this corresponds to an angular dispersion of ~-9512 fs^2 which for 80 cm will lead to an angular dispersion of ϕ_{2a} = ~-11.9 fs^2/mm (which is not

far from the theoretical ϕ_{2a} = -13.3 fs^2/mm); and τ_{in} = ~61.17 fs which is in agreement with the FTL durations already determined. The difference in the GDD values ϕ_{2m} and ϕ_{2c} can be explained as before since the same procedure was used to determine the prism insertion values however since now the prism distance is larger and more dispersion material is inserted with FI the impact of this error is lower than previously and we expect that for larger distances this could be neglected.

The two parameters ϕ_{2m} and ϕ_{2c} give us for the prism insertion value correspondent to the minimum pulse duration (Δx = 15.2 mm) a -16 fs^2 residual GDD which is almost insignificant and thus, once again, we can consider that the value of GDD was compensated using the prism compressor.

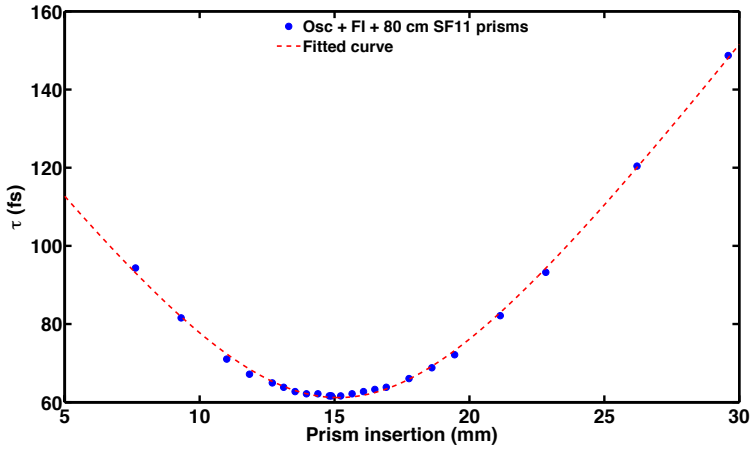

Figure 4.14: Experimental output pulse durations for different values of prism insertion (blue points) and the corresponding fit (red line) to compensate the pulses coming from the oscillator after passing the FI.

5

Extrapolation for the OPCPA system

In order to have an efficient OPCPA system the choice of the appropriate stretcher-compressor assembly is critical and several aspects should be taken into consideration. Worthy to be mentioned is the fact that the efficiency and the bandwidth of an OPCPA are affected by the ratio between the pump and seed pulse durations, and in order to explain it a brief description of the system follows this introduction. Also as the results obtained in the previous chapter show that the behaviour of the main dispersive elements (SF11 prisms, transmission gratings and SF11 rod) are in accordance with the theoretical models at 1030 nm, which provides a good framework for the operation at 900 nm, we end this work with the parameters for which this devices could lead to a successfully compression of both GDD and TOD.

5.1 Optical parametric chirped pulse amplification

The OPCPA setup (Figure 5.1)[21] is seeded by the Coherent Mira 900F oscillator operating at 1030 nm, which provides few nJ pulses at a repetition rate of 76 MHz. These pulses are selected by a 10 Hz pulse picker and injected into a compact chirped volume Bragg grating (CVBG) in a double-pass configuration for stretching. The nJ chirped pulses are then directed to a diode-pumped ytterbium-doped calcium fluoride (Yb:CaF_2) regenerative amplifier where they are amplified up to 3 mJ. After the amplification the pulses are split in two parts: 80% of the pulse is sent again to the CVBG for compression, providing a pulse with 1 mJ and 400 fs[60] and the remaining 20% are sent to the multipass amplifier. This amplifier consists in a 8-pass geometry with ytterbium-doped yttrium aluminium garnet (Yb:YAG) crystal as gain medium, pumped by a high power diode stack with a repetition rate of 1 Hz, raising the energy up to 100 mJ.[61] These pulses, with 150 ps duration, are sent to a frequency-doubling potassium dideuterium phosphate (DKDP) crystal (generating light 515 nm, in the green region) and then used for pumping the two YCOB OPA stages[62]. For the signal pulse, the CPA compressed pulses are

focused in a sapphire block, generating a white light continuum (WLC),[63,64] extending from 600 to 1000 nm. Previous measurements for the amplification in the two YCOB crystals led to output energy about 300 μJ with a broadband spectrum centered at 900 nm and extending over 150 nm.

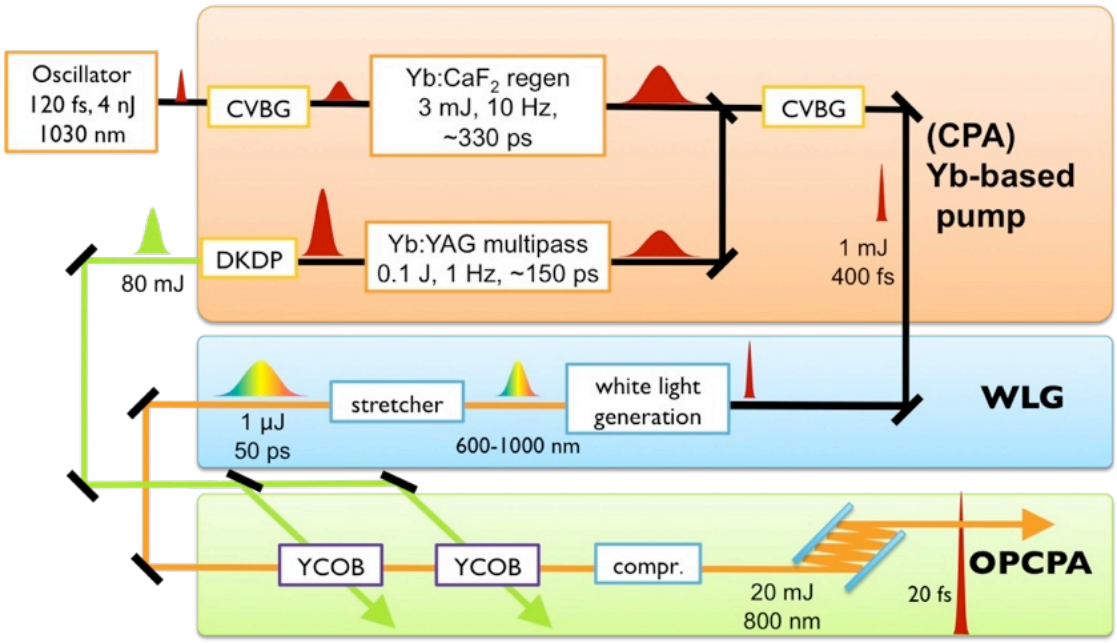

Figure 5.1: Global layout of ultrabroadband OPCPA system. Top box: CPA pump laser based on a double-stage, diode pumped CPA system; middle box: generation of signal pulse based on white light continuum generation (WLG) in bulk media; bottom box: double stage OPCPA system based on YCOB.[21]

5.2 Seed and pump pulses

As we are trying now to improve the efficiency of the OPCPA, stretching the seed pulse to match its duration with that of the pump is of crucial importance. In fact, the greater the overlap is between the two pulses the greater will be the efficiency of the system, as more pump energy will be used. Thus, the seed pulse must be stretched from the femtosecond level to a few picoseconds (or even nanoseconds) depending on the pump pulse length, before the parametric amplification (Figure 5.2). However, as the pump pulses have typically Gaussian profiles, the wings of the seed will experience less gain as compared to the central part, causing a gain-induced bandwidth narrowing (Figure 5.2). Therefore a compromise must be found between bandwidth and efficiency, and for first model and tests the chosen ratio between the seed and pump was of approximately 0.4.[9]

In our case the pump duration of 150 ps after passing through the DKDP, which has an efficiency of ~30%, is ~50 ps meaning that we must stretch the 400 fs seed pulse leaving the regenerative amplifier to ~20 ps. Considering the operation wavelength of the OPCPA at 900 nm and a bandwidth of 150 nm and that we have a Gaussian pulse

this will correspond to an FTL pulse of $\Delta t = 8$ fs (or $\tau = 6.8$ fs). Stretching this pulse to 20 ps will require three passes in the 12.5 cm SF11 glass block.

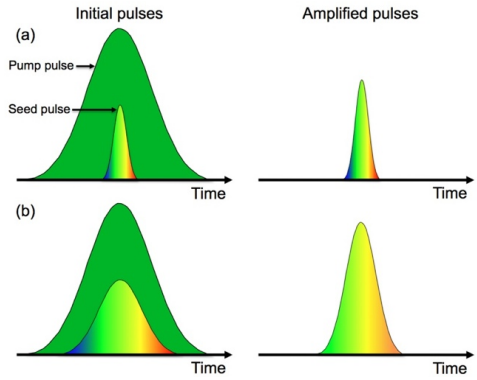

Figure 5.2: Illustration of the effect on efficiency and amplified bandwidth on OPCPA caused by the pump and seed pulse duration ratio. (a) large ratio, allowing bandwidth preservation, but low efficiency; (b) small ratio, allowing high efficiency but bandwidth narrowing.[9]

5.3 Stretcher-compressor assembly

The second important consideration in the stretcher-compressor assembly is to compress the pulses to the intended duration of 20 fs after the amplification. The higher the GDD and TOD inserted by the stretcher the harder it will be to achieve cancellation of the two dispersion orders within a compact setup. In fact, in order to achieve this duration even a residual GDD of 10^2 fs^2 or a TOD of 10^3 fs^3 could have some impact in the pulse. Since SF11 is a highly dispersive material this will mean that large values of TOD and GDD will be introduced even considering that it has a relatively low TOD/GDD ratio, requiring a combination of two compressors:

- the 300 g/mm grating pair, in order to compensate the large amount of GDD within a small and comfortable distance between gratings but at the same time introducing less amount of TOD when compared with that introduced by gratings with higher groove density;
- the SF11 prism compressor, since we need not only to cancel the TOD (which could be achieved with a prism compressor of any material), but we also need it to be a highly dispersive one since a large positive value of TOD is inserted by the SF11 rod and the grating.

Computation of the GDD and TOD values showed that the optimum parameters for achieving the intended compression are a 10.6 cm perpendicular distance between gratings, considering a blazed angle of 32°, and an apex-to-apex distance of 189.3 cm between SF11 prisms with an apex angle of 59° (Table 5.1). An additional simulation was performed considering 3 cm of material insertion in the SF11 prisms, slightly increasing the distances to 11.6 cm between the gratings and to 201.8 cm between the prisms. Al-

though the distance between gratings is within the acceptable range for a compact setup, the distance between the prisms is in the limit of an acceptable compressor size, even using parallel mirrors between them. Note that we are using a ratio of 0.4 for first tests but if we chose to improve the efficiency to a ratio of 0.6, or even if we replace the DKDP crystal by a more efficient one leading to a longer pump pulse duration, a larger stretcher will be required, leading to longer distances between prisms and an increase in the prism compressor size (e.g. when we inserted the 3 cm of material dispersion this led to an increase of 9.4% between gratings and 6.6% between prisms).

Table 5.1: GDD and TOD calculated for pulse stretching and compression of the pulse.

Main optical devices (λ_0 = 900 nm and $\Delta\lambda$ = 150 nm)		ϕ_2 (fs^2)	ϕ_3 (fs^3)
Stretcher	SF11 glass block (3 passes = 37.5 cm)	+60203	+45922
Compressors	300 g/mm transmission grating pair ($\gamma = 32^o$ and L_g = 10.6 cm)	-27255	+36185
	SF11 Brewster prism pair (apex angle = 59^o and L_p = 189.3 cm)	-32920	-82899
Net TOTAL	–	28	-792

6

Conclusions and future work

In the present work we have determined the dispersion parameters caused by the optical elements for pulse stretching and compression in a broadband OPCPA laser amplifier. The obtained dispersion values at a central wavelength of 1030 nm were: for the grating compressor of ~-374.6 fs^2/mm and ~538.5 fs^3/mm; for the SF11 glass of ~154.8 fs^2/mm and ~142.7 fs^2/mm from two different models; for the angular prism dispersion using the first method of ~-6.6 fs^2/mm and using the second of ~-11.9 fs^2/mm; finally the FTL pulses were determined to be between ~51.85 fs and ~61.98 fs.

Through this process we came to several important conclusions as:

- the importance of knowing the chirp of the pulses at the output of the oscillator and thus to characterize the dispersion inside the cavity since it will have an impact in the determination of the intended results (we determined ~97.9 fs^2/mm for the prism material which matches with the SF10 within the error and ~-1888 fs^2 of total GDD for the pulses coming from the cavity). Also it proved the capability of the oscillator in delivering pulses with FTL duration at 1030 nm between ~52 and ~62 fs;
- the need to perform autocorrelations closer to the FTL durations since the precision of these measurements (10% of error associated) is higher at this region leading us to change the experimental approach of studying individually each optical element but instead use a stretcher-compressor assembly with the minimum number of optical devices possible;
- the available data for the TGG Faraday rotator is scarce and we could only make a prediction of the GDD and TOD generated by the FI, which differs from the experimental value (~7078 fs^2);
- although the impact of the TOD was not significant for the majority of the experimental setups while using FTL pulses of these durations situated between ~52 and ~62 fs, for the study of gratings with two passes in the SF11

rod the third order proved to be already visible and important while computing the dispersions and durations of the pulses (the TOD was determined to be at the minimum output pulse duration of ~76974 fs^3);

- also we detected that some mirrors are not appropriate at all to use in the setup where is extremely important to have a high control of the dispersion introduced by components that are not the main dispersive elements;
- finally, discrepancies in the values for the prisms compressor are probably due to imprecision in the values required in order to calculate the material insertion and that as larger is the stretcher-compressor inserting more material and angular dispersion the lower will be the impact of this error.

Extrapolation of the experimental results to 900 nm central wavelength and other parameters of the OPCPA pulses (such as duration of the pump and signal) proved that the devices chose for the stretcher-compressor assembly will achieve its purpose at the boundary of the acceptable range, since a 2 m wide prism compressor would be required to compensate the TOD introduced by the long length of SF11 and the gratings.

6.1 Future work

In future work it would be interesting to replace some dispersive elements in order to achieve the intended compact stretching-compressor assembly. From data sheets of SCHOTT for optical glass[65] rather then DOM we compare SF11 with a relatively higher dispersive material that is SF57 that has the important advantage of inserting lower TOD values (low TOD/GDD). Also we compare GDD and TOD introduced by SF11 prism with a recent material that is one of the most dispersive elements transparent to the wavelength we are working that is N-SF66 which will probably reduce the prism compressor size in more than 1 m.[65]

Table 6.1: Comparison between the GDD and TOD introduced per mm by the current optical elements for stretching and compressing the pulses with an even higher dispersive alternative.

	Current optical elements			Alternative optical elements		
$\lambda_0 = 900$ nm	ϕ_2 (fs^2/mm)	ϕ_3 (fs^3/mm)	TOD/GDD	ϕ_2 (fs^2/mm)	ϕ_3 (fs^3/mm)	TOD/GDD
Transparent material	SF11			SF57		
	157.2	119.9	0.76	187.8	130.7	0.70
Grating pair	300 g/mm (31.7°)			300 g/mm (31.7°)		
	-257.1	341.4	1.33	-257.1	341.4	1.33
Prism pair	SF11			N-SF66		
	-17.4	-43.8	2.52	-35.3	-83.4	2.36

References

[1] W. Koechner, "Solid-State Laser Engineering," *Springer Science and Business Media*, New York (2006)

[2] D. Strickland and G. Mourou, "Compression of amplified chirped optical pulses," *Opt. Commun.* **55**(6), 447-449 (1985)

[3] T. Brabec and F. Krausz, "Intense few-cycle laser fields: Frontiers of nonlinear optics," *Rev. Mod. Phys.* **72**, 545-591 (2000)

[4] T. Seggebrock et al., "The Pulse Intensity-Duration Conjecture: Evidence from free-electron lasers," *Prog. Theor. Exp. Phys.* 013A02 (2014)

[5] S. Backus et al., "High power ultrafast lasers," *Rev. Sci. Instrum.* **69**, 1207-1223 (1998)

[6] J. D. Kafka et al., "Picosecond and femtosecond pulse generation in a regeneratively Kerr-lens mode-locked Ti:sapphire laser," *IEEE J. Quantum Electron.* **28**(10), 2151-2162 (1992)

[7] X. Lu et al., "Trends in ultrashort and ultrahigh power laser pulses based on optical parametric chirped pulse amplification," Chin. Phys. B **24**(1) (2015)

[8] F. Tavella, "Multiterawatt few-cycle pulse OPCPA for applications in high-field physics," Max Planck Institute of Quantum Optics (2008)

[9] L. P. Ramirez, "Few-cycle OPCPA laser chain," PhD Thesis, Université Paris-Sud (2013)

[10] S. Witte and K. S. E. Eikema, "Ultrafast optical parametric chirped-pulse amplification," *IEEE J. Sel. Topics Quantum Electron.* **18**(1), 296-307 (2012)

[11] A. Dubietis, R. Butkus, and A. P. Piskarskas, "Trends in chirped pulse optical parametric amplification," *IEEE J. Sel. Topics Quantum Electron.* **12**(2), 163-172 (2006)

[12] R. Butkus et al., "Progress in chirped pulse optical parametric amplifiers," *Appl. Phys. B* **79**(6), 693-700 (2004)

[13] A. Vaupel et al., "Concepts, performance review, and prospects of table-top, few-cycle optical parametric chirped-pulse amplification," *Opt. Eng.* **53**(5), 051507 (2013)

[14] G. Cerullo and S. De Silvestri, "Ultrafast optical parametric amplifiers," *Rev. Sci. Instrum.* **74**(1), 1-18 (2003)

[15] D. Herrmann et al., "Generation of sub-three-cycle, 16 TW light pulses by using noncollinear optical parametric chirped-pulse amplification," *Opt. Lett.* **34**(16), 2459-2461 (2009)

[16] J. Rothhardt et al., "Octave-spanning OPCPA system delivering CEP-stable few-cycle pulses and 22 W of average power at 1 MHz repetition rate," *Opt. Express* **20**(10), 10870-10878 (2012)

[17] A. Klingebiel et al., "High energy picosecond Yb:YAG CPA system at 10 Hz repetition rate for pumping optical parametric amplifiers," *Opt. Express* **19**(6), 5357-5363 (2011)

[18] S. Witte et al., "Generation of few-cycle terawatt light pulses using optical parametric chirped pulse amplification," *Opt. Express* **13**(13), 4903-4908 (2005)

[19] V.V. Lozhkarev et al., "200 TW 45 fs laser based on optical parametric chirped pulse amplification," *Opt. Express* **14**(1), 446-454 (2006)

[20] Z. Liao et al., "Energy and average power scalable optical parametric chirped-pulse amplification in yttrium calcium oxyborate," *Opt. Lett.* **31**(9), 1277-1279 (2006)

[21] G. Figueira et al., "Generation of ultrabroadband energetic laser pulses by noncollinear optical parametric chirped pulse amplification," *Proc. SPIE* **8785**, 87850T (2013)

[22] G. Figueira, "Development and characterisation of a Ti:sapphire - Nd:glass laser system based on chirped pulse amplification", PhD Thesis, Technical University of Lisbon (2001)

[23] A. Monmayrant et al., "A newcomer's guide to ultrashort pulse shaping and characterization," *J. Phys. B: At. Mol. Opt. Phys.* **43**(10), 103001 (2010)

[24] TM. Wollenhaupt, A. Assion and T. Baumert, "Femtosecond Laser Pulses: Linear Properties, Manipulation, Generation and Measurement – Springer Handbook of Lasers and Optics," *F. Träger, Springer Science and Business Media*, New York (2007)

[25] M. A. Amorim, "High-power and tuneable ultrashort laser pulses in the sub-two-cycle regime: towards novel light sources", PhD Thesis, University of Porto (2012)

[26] V. Chauhan, "Pulse compression and dispersion control in ultrafast optics," PhD Thesis, Georgia Institute of Technology (2010)

[27] J. Zhou et al., "Generation of 21-fs millijoule-energy pulses by use of Ti:sapphire," *Opt. Lett.* **19**(2), 126-128 (1994)

[28] M. Hemmer, "Few-cycle pulses amplification for attosecond science applications: modelling and experiments," PhD Thesis, University of Central Florida (2005)

[29] M. N. Polyanskiy, "Refractive index database," *http://refractiveindex.info*

[30] E. B. Treacy, "Optical pulse compression with diffraction gratings," *IEEE J. Quantum Electron.* **5**(9), 454–458 (1969)

[31] Thorlabs Inc., "NIR Transmission Gratings," *www.thorlabs.com*

[32] R. L. Fork, O. E. Martinez, and J. P. Gordon, "Negative dispersion using pairs of prisms," *Opt. Lett.* **9**(5), 150-152 (1984)

[33] Thorlabs Inc., "Angle of Minimum Deviation Through a Prism," *www.thorlabs.com*

[34] P. Dombi et al., "Pulse compression with time-domain optimized chirped mirrors," *Opt. Express* **13**(26), 10888-10894 (2005)

[35] R. Szipöcs and A. Koházi-Kis, "Theory and design of chirped dielectric laser mirrors," *Appl. Phys. B* **65**(2), 115-135 (1997)

[36] J.-H. Son, "Terahertz Biomedical Science and Technology," *CRC Press, Taylor & Francis Group*, Florida (2014)

[37] Layertec – optische Beschichtungen GmbH, "Introduction to Femtosecond Laser Optics," *https://www.layertec.de*

[38] C. H. Brito Cruz, P. C. Becker, R. L. Fork, and C. V. Shank, "Phase correction of femtosecond optical pulses using a combination of prisms and gratings," *Opt. Lett.* **13**(2), 123-125 (1988)

[39] I. A. Walmsley and C. Dorrer, "Characterization of ultrashort electromagnetic pulses," *Adv. Opt. Photon.* **1**(2), 308-437 (2009)

[40] R. Trebino et al., "Measuring ultrashort laser pulses in the time-frequency domain using frequency-resolved optical gating," *Rev. Sci. Instrum.* **68**(9), 3277-3295 (1997)

[41] E. P. Ippen and C. V. Shank, "Techniques for Measurement – Ultrashort Light Pulses ," Springer-Verlag, **18**, 83-122 (1977)

[42] M. Maier, W. Kaiser and J. A. Giordmaine, "Intense light bursts in the stimulated raman effect," *Phys. Rev. Lett.* **17**(26), 1275-1277 (1966)

[43] Swamp Optics, "Custom Pulse-Measurement Devices," *http://www.swampoptics.com*

[44] A. Baltuska et al., "Amplitude and phase characterization of 4.5-fs pulses by frequency-resolved optical gating," *Opt. Lett.* **24**(8), 569-571 (1999)

[45] Rick Trebino, "Ligth-Pulse-Measurement Tutorial," *http://www.frog.gatech.edu*

[46] C. H. Brito Cruz et al., "Phase correction of femtosecond optical pulses using a combination of prisms and gratings," *Opt. Lett.* **13**(2), 123-125 (1987)

[47] Craig Siders, "Disperse-O-Matic," *http://www.linkedin.com/in/craigsiders*

[48] Biophtonic Solutions Inc., "*femto*Pulse Master," *http://www.biophotonicsolutions.com*

[49] A·P·E Angewandte Physik & Elektronik GmbH, "Dispersion Calculator," *http://www.ape-berlin.de*

[50] Leysop Ltd., "Faraday Optical Isolators," *http://www.leysop.com*

[51] Leysop Ltd., "Glan-Taylor Calcite Air Spaced Polarizer," *http://www.leysop.com*

[52] Spectrogon, "Grating design tool," *http://www.spectrogon.com*

[53] EKSMA Optics, "Laser Dispersing Prisms," *http://eksmaoptics.com*

[54] Tektronix, "Oscilloscopes," *www.tek.com*

[55] Ocean Optics Inc., "Modular Spectrometers," *oceanoptics.com*

[56] Coherent Inc., "Mira 900," *www.coherent.com*

[57] Q. Chen et al., "Reflected second-harmonic generation with coupled surface-plasmon modes in Ag/liquid/Ag layers," *J. Opt. Soc. Am. B* **16**(6), 971-975 (1999)

[58] U. Schlarb and B. Sugg, "Refractive Index of Terbium Gallium Garnet," *Phys. Stat. Sol. (b)* **182**(2), K91-K93 (1994)

[59] Shanghai optics, "TGG," *www.shanghai-optics.com*

[60] C. P. João et al., "Dispersion compensation by two-stage stretching in a sub-400 fs, 1.2 mJ Yb:CaF_2 amplifier," *Opt. Express* **22**(9), 10097-10104 (2014)

[61] C. P. João et al., "Hybrid Yb:CaF_2/Yb:YAG compact CPA laser generating 100 mJ for pumping a broadband OPA," *II International Conference on Applications of Optics and Photonics*, Aveiro (2014)

[62] H. Pires e tal., "Numerical evaluation of ultrabroadband parametric amplification in YCOB," *J. Opt. Soc. Am. B* **31**(11), 2608-2614 (2014)

[63] J. M. Dudley, G. Genty and S. Coen, "Supercontinuum generation in photonic amplifiers," *Rev. Mod. Phys.* **78**(4), 1135-1184 (2006)

[64] T. Imran and G. Figueira, "Intensity-phase characterization of white-light continuum generated in sapphire by 280 fs laser pulses at 1053 nm," *J. Opt. A-Pure Appl. Op.* **14**, 035201 (2012)

[65] SCHOTT Inc., "Data sheets – Optical Glass," *http://www.schott.com*